The impact of snow nitrate photolysis on boundary layer chemistry and the recycling and redistribution of reactive nitrogen across Antarctica in a global chemical transport model

Zatko, M.C.[1], Geng, L.[1], Alexander, B. [1], Sofen, E.D.[2], Klein, K.[3]

[1]Department of Atmospheric Sciences, University of Washington, Seattle, United States
[2]Department of Chemistry, University of York, York, United Kingdom
[3]Division of Glaciology, Alfred Wegener Institute Helmholtz Centre for Polar and Marine Research, Bremerhaven, Germany

Correspondence to Becky Alexander (beckya@uw.edu)

Abstract

The formation and recycling of reactive nitrogen (NO, NO_2, HONO) at the air-snow interface has implications for air quality and the oxidation capacity of the atmosphere in snow-covered regions. Nitrate (NO_3^-) photolysis in snow provides a source of oxidants (e.g., hydroxyl radical) and oxidant precursors (e.g., nitrogen oxides) to the overlying boundary layer, and alters the concentration and isotopic (e.g., $\delta^{15}N$) signature of NO_3^- preserved in ice cores. We have incorporated the photolysis of Antarctic snow NO_3^- into a global chemical transport model (GEOS-Chem) to examine the implications of snow NO_3^- photolysis for boundary layer chemistry, the recycling and redistribution of reactive nitrogen across the Antarctic continent, and the preservation of ice-core NO_3^- in Antarctic ice cores. This modeling framework uses an idealized snowpack that accounts for the spatial variability in parameters that influence snow NO_3^- photolysis. The goal of this research is to investigate the potential spatial variability of snow-sourced NO_x fluxes along with the recycling, loss, and areal redistribution of nitrogen across Antarctica, which is an environment in which observations of these parameters over large spatial scales are difficult to obtain. The calculated potential fluxes of snow-sourced NO_x in Antarctica range from 0.5 $x10^8$ to $7.8x10^8$ molec cm^{-2} s^{-1} and calculated e-folding depths of UV actinic flux in snowpack range from 24 to 69 cm. Snow-sourced NO_x increases mean austral summer boundary layer mixing ratios of total nitrate (HNO_3+NO_3^-), NO_x, OH, and O_3 in Antarctica by a factor of up to 32, 38, 7, and 2, respectively, in the model. Model results also suggest that NO_3^- can be recycled between the air and snow multiple times and that NO_3^- can remain in the snow photic zone for at least 7.5 years on the East Antarctic plateau. The fraction of photolysis-driven loss of NO_3^- from the snow is roughly -0.99 on the East Antarctic plateau, while areas of wind convergence (e.g., over the Ronne Ice Shelf) have a net gain of NO_3^- due to redistribution of snow-sourced reactive nitrogen across the Antarctic continent. The modeled enrichment in ice-core $\delta^{15}N(NO_3^-)$ due to photolysis-driven loss of snow NO_3^- ranges from 0‰ to 363‰, with the largest enrichments on the East Antarctic plateau. There is a strong relationship between the degree of photolysis-driven loss of snow NO_3^- and the degree of nitrogen recycling between the air and snow in regions of Antarctica with a snow accumulation rate greater than 85 kg m^{-2} a^{-1} in the present day. This modeling framework study is also used to perform a variety of sensitivity studies to highlight the largest uncertainties in our ability to model these processes in order to guide future lab and field campaigns.

Maria Zatko 9/12/15 7:51 AM
Deleted: , ozone… and oxidant precu… [1]

Maria Zatko 9/4/15 12:44 PM
Formatted: Not Superscript/ Subscript

Maria Zatko 9/4/15 12:44 PM
Deleted: NO3-

Maria Zatko 9/4/15 12:44 PM
Formatted: Not Superscript/ Subscript

Maria Zatko 9/4/15 12:44 PM
Deleted: NO3-…photolysis for bound… [2]

Maria Zatko 9/4/15 12:44 PM
Formatted … [3]

Maria Zatko 9/4/15 12:44 PM
Deleted: …he calculated potential flu… [4]

Maria Zatko 10/16/15 5:36 PM
Formatted … [5]

Maria Zatko 9/4/15 12:20 PM
Deleted: , suggesting that ice-core $\delta^{15}N(NO_3^-)$ observations can be used to assess the degree of nitrogen recycling and loss over much of Antarctica and aid in the interpretation of ice-core NO_3^- in terms of past atmospheric variability of reactive nitrogen.

1. Introduction

Nitrogen oxides (NO_x=NO+NO_2) emitted from fossil fuel combustion, biomass burning, soil microbial activity, and lightning have adverse respiratory effects, contribute to the formation of atmospheric acidity, and are a key ingredient in tropospheric oxidant cycling leading to the formation of ground-level ozone (O_3). Ozone also has adverse respiratory effects, is an effective greenhouse gas [*UNEP*, 2011], and its photolysis dominates hydroxyl radical (OH) production in much of the troposphere [*Thompson*, 1992]. Oxidation to form nitrate (HNO_3/NO_3^-) is the main sink for NO_x in the troposphere [*Logan*, 1983], and the lifetime of NO_x against oxidation to nitrate is 1-3 days in polar regions [*Levy et al.*, 1999]. NO_3^- is lost from the atmosphere through dry and wet deposition to the Earth's surface, and has an atmospheric lifetime of roughly 5 days [*Xu and Penner*, 2012]. In Antarctica, NO_3^- deposited to the snowpack originates from both the troposphere (e.g., long-range transport) [*Lee et al.*, 2014] and stratosphere [*Frey et al.*, 2009, *Savarino et al.*, 2007]. In snow-covered regions, the deposition of NO_3^- is not a permanent sink for NO_x, as the photolysis of snow NO_3^- returns reactive nitrogen (N_r=NO_x, HONO) back to the atmosphere, with implications for other oxidants such as OH and ozone [*Domine and Shepson,* 2002].

Snow photochemistry significantly influences boundary layer chemistry and plays an important role in oxidant production and cycling, especially in pristine regions, such as Antarctica [*Bloss et al.*, 2007, *Chen et al.*, 2004, *Grannas et al.*, 2007, *Helmig et al.*, 2008]. Snow photochemistry may have more widespread impacts since up to 40% of land on Earth is snow-covered at a given time [*Grannas et al.*, 2007]. NO_3^- is not the only photochemically-active species in snow. The photolysis of nitrite (NO_2^-) in snow and the photolysis of snow-sourced formaldehyde (CH_2O), nitrous acid (HONO), and hydrogen peroxide (H_2O_2) provide additional sources of N_r and OH to the boundary layer. Bromine (Br_2) is also produced in the snow via reactions involving bromide (Br^-), photochemically-active species (e.g., NO_3^-), and photochemically-produced species (e.g., OH) within snow grains [*Pratt et al.*, 2013].

In snow, NO_3^- photolysis likely occurs in the liquid-like region (LLR) on the surface of ice grains, in cracks between ice grains, or in brine pockets embedded within ice grains [*Domine et al.*, 2013]. There are two channels for NO_3^- photolysis at wavelengths (λ)=290-345 nm. In the aqueous phase, NO_3^- can photolyze to produce NO_2 and OH (E1), or produce NO_2^- and $O(^3P)$ (E2), but E1 is the dominant pathway [*Grannas et al.*, 2007, *Mack and Bolton*, 1999, *Meusinger et al.*, 2014].

$$NO_3^-(aq) + h\nu(+H^+) \rightarrow NO_2(aq) + OH(aq), \quad \text{E1}$$

$$NO_3^-(aq) + h\nu \rightarrow NO_2^-(aq) + O(^3P)(aq), \quad \text{E2}$$

The aqueous phase NO_2 produced in E1 is can be transferred to the gas phase and subsequently transported into the interstitial air [*Boxe et al.,* 2005] and then released to the atmosphere. The quantum yield (ϕ) in E1 is strongly influenced by the location of NO_3^- in an ice grain. Chu and Anastasio [2003] froze NO_3^--doped water in the lab and measured the quantum yield for E1 (0.003 molec photon^{-1} at T=253K) as frozen ice grains were exposed to ultraviolet (UV) radiation. Zhu et al. [2010] deposited HNO_3 on

Maria Zatko 9/12/15 9:46 AM
Deleted: on the order of one day

Maria Zatko 9/12/15 10:21 AM
Deleted: on the order of several

Maria Zatko 9/12/15 10:21 AM
Deleted: *Logan*

Maria Zatko 9/12/15 10:21 AM
Deleted: 1983

Maria Zatko 9/12/15 10:25 AM
Deleted: recycles

Maria Zatko 9/8/15 11:18 AM
Deleted: partially

Maria Zatko 9/8/15 11:19 AM
Deleted: , NO_2(g), during transport from the LLR to the interstitial air

Maria Zatko 9/8/15 11:44 AM
Deleted: 3x10-3

Maria Zatko 9/8/15 11:50 AM
Deleted: 53

an ice film and measured ϕ for E1 (0.6 molec photon^{-1} at T=253K), as the frozen surface was irradiated with UV radiation. In a recent study by Meusinger et al. [2014], ϕ=0.003-0.44 molec photon^{-1} for E1, which nearly spans the full range of previously reported quantum yields. Results from Meusinger et al. [2014] suggest that ϕ is dependent on the length of time that snow is exposed to UV radiation, as well as the location of NO_3^- in the ice grain. Meusinger et al. [2014] suggest that two photochemical domains of NO_3^- exist: photolabile NO_3^- and NO_3^- buried within the ice grain. The NO_x produced from the photolysis of photolabile NO_3^- can escape the ice grain, while the NO_x produced from the photolysis of buried NO_3^- is likely to undergo recombination chemistry within the snow grain, thus lowering the quantum yield of NO_x for NO_3^- photolysis.

The NO_2^- produced in E2 is quickly photolyzed at longer wavelengths (λ=290-390 nm) in the LLR or can react with OH or H^+ in the LLR to produce N_r [*Grannas et al.*, 2007]:

$$NO_2^-(aq) + h\nu(+H^+, aq) \rightarrow NO(aq) + OH(aq), \quad \text{E3}$$
$$NO_2^-(aq) + OH(aq) \rightarrow NO_2(aq) + OH(aq), \quad \text{E4}$$
$$NO_2^-(aq) + H^+(aq) \rightarrow HONO(aq), \quad \text{E5}$$

HONO produced in E5 can rapidly photolyze to produce NO and OH in the interstitial air or the atmospheric boundary layer [*Anastasio and Chu*, 2009]. Reactions involving NO_2^- are intermediate reactions for NO_3^- photolysis because NO_3^- photolysis is required for NO_2^- formation and the end products of E1-E5 are all N_r. Once emitted, NO_2 and NO are efficiently transported to the overlying atmosphere via windpumping [*Zatko et al.*, 2013] and enter into rapid NO_x-cycling reactions. In the atmosphere, the relative abundance of NO and NO_2 will be determined by local atmospheric conditions, specifically oxidant concentrations (e.g., O_3, HO_2, RO_2, BrO, and ClO) [*Frey et al.,* 2013]. The snow-sourced NO_x is then re-oxidized to HNO_3 via E6 under sunlit conditions.

$$NO_2(g) + OH(g) \rightarrow HNO_3(g), \quad \text{E6}$$

The HNO_3 produced in E6 can undergo wet or dry deposition to the snow surface [*Dibb et al.*, 2004] within a day [*Slusher et al.*, 2002, *Wang et al.*, 2008]. Evidence for HNO_3 re-deposition is seen in the snow NO_3^- concentration profile at many polar locations, where NO_3^- concentrations are at least an order of magnitude higher in the top two centimeters (cm) of snow compared to NO_3^- concentrations below [*Dibb et al.*, 2004, *Frey et al.*, 2009, *Mayewski and Legrand*, 1990, *Rothlisberger et al.*, 2000]. Once HNO_3 is deposited back to the snow, it is available for photolysis again. NO_3^- can be recycled multiple times between the boundary layer and the snow before burial below the photic zone [*Davis et al.*, 2008, *Erbland et al.*, 2015].

The photolysis of snow NO_3^- and subsequent recycling between the air and snow alters the concentration and isotopic (e.g., $\delta^{15}N$) signature of NO_3^- that is ultimately preserved in polar ice sheets, which hampers the interpretation of ice-core NO_3^- records [*Wolff et al.*, 2008]. Such records have been sought to reconstruct the past history of the abundance of NO_x in the atmosphere [*Wolff*, 1995]. It has also been suggested that the nitrogen ($\delta^{15}N$) and oxygen ($\Delta^{17}O = \delta^{17}O - 0.52\times\delta^{18}O$) isotopic composition of ice-core NO_3^- can

Maria Zatko 9/8/15 12:09 PM
Deleted: spans the range of

Maria Zatko 9/12/15 8:21 AM
Deleted: disturbs the preservation of NO_3^-

Maria Zatko 9/12/15 8:22 AM
Deleted: and

Maria Zatko 9/12/15 8:22 AM
Deleted: concentration

provide information on past variability in atmospheric NO_x sources and oxidant abundances [e.g., *Alexander et al*., 2004, *Hastings et al*., 2005]. Different sources of NO_x have different $\delta^{15}N$ signatures (~ -19‰ to 25‰, see summary in *Geng et al*., 2014a), giving ice-core $\delta^{15}N(NO_3^-)$ measurements the potential to track NO_x-source changes over time. The oxygen-17 excess of NO_3^- ($\Delta^{17}O(NO_3^-)$) is determined mainly by the relative abundance of the oxidants involved in NO_x cycling and conversion of NO_2 to NO_3^- (i.e. O_3, HO_2, RO_2, OH), giving ice-core $\Delta^{17}O(NO_3^-)$ measurements the potential to track variability in the relative abundance of these oxidants over time. However, $\delta^{15}N(NO_3^-)$ and $\Delta^{17}O(NO_3^-)$ in ice cores can also be influenced by post-depositional processing of snow NO_3^- initiated by photolysis. In this study we focus on the impact of snow NO_3^- photolysis on ice-core $\delta^{15}N(NO_3^-)$.

Ice-core $\delta^{15}N(NO_3^-)$ values will be altered if there is photolysis-driven loss of NO_3^- from the snow when snow-sourced NO_x is transported away from the site of primary deposition. Nitrate photolysis in snow is associated with a large fractionation constant (ε) of -47.9‰ [*Berhanu et al*., 2014], providing the boundary layer with a source of NO_x that is highly depleted in $\delta^{15}N$, leaving highly enriched $\delta^{15}N(NO_3^-)$ in the snow. In the Weddell Sea, atmospheric $\delta^{15}N(NO_3^-)$ values are as low as -40‰, indicating transport of snow-sourced NO_x from the continental interior [*Morin et al*., 2009], while on the East Antarctica plateau, snow $\delta^{15}N(NO_3^-)$ up to 480‰ has been reported [*Blunier et al*., 2005, *Erbland et al*., 2013, *Frey et al*., 2009, *Shi et al.,* 2014], indicating net loss of NO_3^- driven by photolysis. If snow-sourced NO_x is simply re-deposited back to the snow surface at the site of emission, a vertical profile in $\delta^{15}N(NO_3^-)$ within the snow photic zone will develop due to vertical redistribution of NO_3^- [*Erbland et al*., 2013, *Frey et al*., 2009]; however, the depth-integrated $\delta^{15}N(NO_3^-)$ will not be impacted, even with active photolysis-driven recycling between the atmosphere and the snow. Enrichment in $\delta^{15}N(NO_3^-)$ in ice cores requires photolysis-driven loss from snow combined with atmospheric transport of the resulting NO_x. In addition to photolysis, ice-core $\delta^{15}N(NO_3^-)$ values are also influenced by evaporation of HNO_3 [*Mulvaney et al*., 1998] from snow and by atmospheric processing, such as NO_x cycling [*Freyer et al*., 1993] and gas-particle partitioning [*Heaton et al*., 1997, *Geng et al*., 2014a]; however, these impose a fractionation in $\delta^{15}N(NO_3^-)$ at least an order of magnitude smaller than photolysis, and are thus not able to explain the large enrichments in snow $\delta^{15}N(NO_3^-)$ observed on the East Antarctic plateau [*Blunier et al*., 2005, *Erbland et al*., 2013, *Frey et al*., 2009, *Shi et al.,* 2014].

Here we incorporate a snowpack actinic flux parameterization used to calculate the photolysis of snow NO_3^- into a global chemical transport model. The idealized Antarctic ice sheet incorporated into GEOS-Chem has similar topography, climate, and weather as the real Antarctic ice sheet, but is subject to assumptions about the chemical and physical properties of the snow. The idealized snowpack in this modeling framework accounts for the spatial variability in parameters important to snow NO_3^- photolysis in order to investigate the potential spatial variability in snow-sourced NO_x fluxes and associated reactive nitrogen recycling and redistribution across Antarctica, where observations of these parameters over large spatial scales are difficult to obtain. The potential impacts of nitrogen recycling between the air and snow on boundary layer chemistry as well as the

Maria Zatko 9/12/15 8:23 AM
Deleted: the preservation of

Maria Zatko 9/4/15 3:50 PM
Deleted: This modeling framework is use

Maria Zatko 9/4/15 1:24 PM
Deleted: d

Maria Zatko 9/4/15 1:28 PM
Deleted: evaluate the

Maria Zatko 9/4/15 1:28 PM
Deleted: impact of a

Maria Zatko 9/4/15 1:28 PM
Deleted: the

impacts of photolysis-driven loss of NO_3^- from the snow on the preservation of ice-core NO_3^- across Antarctica are examined in this study. A major advantage of using a global chemical transport model framework is the ability to examine the redistribution and loss of reactive nitrogen across large spatial scales due to photolysis-driven loss of snow NO_3^-. Section 2 describes the inclusion of a snowpack actinic flux parameterization and NO_3^- photolysis into a global chemical transport model, GEOS-Chem. Section 3 explores the implications of photolysis-driven reactive nitrogen recycling and redistribution for boundary layer chemistry and the alteration of NO_3^- concentration and its isotopes ultimately archived in ice cores. We end by using our model sensitivity studies to highlight the largest uncertainties in our ability to model these processes as a guide for future laboratory and field studies.

2. Methods

2.1. Incorporating Snow NO_3^- Photolysis into a Global Chemical Transport Model

Table 1 provides a glossary of the variables used throughout this paper.

2.1.1. Global Chemical Transport Model Description

GEOS-Chem is a global 3-dimensional (3-D) model of coupled aerosol-oxidant chemistry with detailed HO_x-NO_x-VOC-O_3-BrO_x tropospheric chemistry originally described in Bey et al. [2001]. The model uses assimilated meteorological data from the NASA Goddard Earth Observing System (GEOS-5) including winds, convective mass fluxes, boundary layer depths, temperature, precipitation, and surface properties. Meteorological data have 6-hour temporal resolution (3-hour for surface variables and mixing depths). The TPCORE advection algorithm [*Lin and Rood*, 1996] is the transport routine in GEOS-Chem and is based on the calculation of the slopes between neighboring grid boxes. At the poles, neighboring grid boxes are used to estimate transport of chemical species into and out of the circular polar grid box. The spectral direct and diffuse downwelling surface irradiance and photolysis frequencies are calculated using the Fast-JX radiative transfer module [*Wild et al*., 2000, *Bian and Prather*, 2002, *Mao et al*., 2010]. In GEOS-Chem, aerosols can be wet deposited via scavenging in convective updrafts and by rainout from convective anvils and large-scale precipitation [*Liu et al*., 2001]. The wet deposition scheme for gases is described by Amos et al. [2012] and the scavenging of aerosol by snow and cold/mixed precipitation is described by Wang et al. [2011]. Dry-deposition velocities for coarse mode aerosols (radii between 1-10 mm) are calculated based on aerosol size and hydroscopic growth as described in Zhang et al. [2001]. Aerosol deposition to snow and ice surfaces is described by Fisher et al. [2011]. For smaller aerosols (radii less than 1 μm), dry deposition velocities are calculated with a standard resistance-in-series scheme [*Wang et al*., 1998, *Wesely*, 1989].

Anthropogenic NO_x emissions are from the EDGAR 3.2-FT2000 global inventory for the year 2000 [*Oliver et al*., 2005], scaled by country on the basis of energy statistics as described by van Donkelaar et al. [2008]. The monthly inventory of emissions from biomass burning are from the Global Fire Emissions Database (GFED2) [*van der Werf et al.,* 2009]. Soil NO_x emissions are computed using a parameterization described in Hudman et al. [2012], which is a function of vegetation type, temperature, soil moisture,

Maria Zatko 9/4/15 1:45 PM
Deleted: boundary layer chemistry and

Maria Zatko 9/4/15 1:46 PM
Deleted: the A

Maria Zatko 9/4/15 1:46 PM
Deleted: continent

Maria Zatko 9/4/15 1:37 PM
Deleted: , such as the Antarctic continent,

Maria Zatko 9/12/15 8:26 AM
Deleted: -

Maria Zatko 9/12/15 8:28 AM
Deleted: preservation

precipitation, and fertilizer emissions. Emissions of NO_x from lightning are linked to deep convection following the parameterization of *Price and Rind* [1992] and are scaled globally as described by Murray et al. [2012] to match OTD/LIS climatological observations of lightning flashes. The stratospheric source of NO_y (=NO_x+HNO_3) utilizes monthly climatological 3-D production and loss rates from the Global Modeling Initiative (GMI) model [*Allen et al.*, 2010], which captures the formation of the polar vortex and PSC sedimentation [*Murray et al.*, 2012].

For this work, GEOS-Chem version v9-01-01 was run at 2°x2.5° horizontal resolution with 72 hybrid vertical levels using GEOS-5 meteorology from May 2009 to May 2010. The model was spun up for six months prior to May 2009. There are no sub-surface (snow) layers in GEOS-Chem and the three lowest vertical levels are each roughly 100 meters in height above Antarctica. The boundary layer in GEOS-Chem is calculated using a parameterization involving the bulk Richardson number with surface friction, a turbulent velocity scale, and non-local fluxes of heat and moisture [*Holtslag and Boville*, 1993] as implemented by Lin and McElroy [2010]. The mixing of emissions, dry deposition, and concentrations of individual species within the boundary layer are determined by static instability. In a stable boundary layer, the local scheme based on eddy diffusivity-theory is used, and the mixing is weak. In an unstable boundary layer, boundary layer mixing is triggered by large eddies. Average boundary layer mixing ratios (ppbv) of species reported in this study (e.g., NO_3^-, NO_x, OH, O_3) are mixing ratios in the lowest vertical grid box (total height ~ 100 m).

Figure 1 illustrates the nitrogen recycling associated with snow NO_3^- photolysis as included in the model. The total flux of snow-sourced NO_x from the snow, F_{NOx} (molec cm^{-2} s^{-1}), is calculated using the wavelength-dependent absorption cross-section for NO_3^- photolysis (σ_{NO3}^-, cm^2 $molec^{-1}$), the temperature (T)- and pH-dependent quantum yield for NO_3^- photolysis (ϕ, molec $photon^{-1}$), the depth- and wavelength-dependent actinic flux in the snow photic zone (I, photons cm^{-2} s^{-1} nm^{-1}), and the average NO_3^- concentration ($[NO_3^-]$, molec cm^{-3}) over the depth of integration. F_{NOx} is calculated in E7 and converted into units of ng N m^{-2} yr^{-1} in E8 and E9.

$$F_{NOx} = \int_{\lambda_0}^{\lambda_1} \int_{z_0}^{z_{3e}} \sigma_{NO_3^-}(\lambda) \cdot \phi(T, pH) \cdot I(\lambda, z) \cdot [NO_3^-](z)\, d\lambda\, dz, \quad \text{E7}$$

In E7, σ_{NO3}^- is from Burley and Johnston [1992]. The quantum yield from Chu and Anastasio [2003] assuming T=244K and pH=5 is used for the base case scenario and ϕ from Zhu et al. [2010] is used for sensitivity studies. The actinic flux (I) is integrated from the snow surface (z_0) to the depth of the photic zone (z_{3e}). The snow photic zone is defined as three times the e-folding depth of ultraviolet (UV) actinic flux in snow (z_{3e}), where 1 e-folding depth is z_e. Below z_{3e}, more than 95% of the radiation has been attenuated and minimal photochemistry occurs. The flux of snow-sourced NO_x is integrated over several ultraviolet wavelength bands (298-307 nm, 307-312 nm, 312-320 nm, 320-345 nm), which are then summed to calculate total F_{NOx} from the photolysis of snow NO_3^- between λ=298-345 nm. We assume that all NO_x formed in E7 is immediately desorbed into the gas-phase and transported from the LLR to the interstitial air and then into the overlying boundary layer [*Zatko et al.*, 2013].

Maria Zatko 10/13/15 4:19 AM
Deleted: The calculated boundary layer mixing ratios are insensitive to whether the average mixing ratios in the lowest grid box (total height ~ 100 m) or the three lowest grid boxes (total height ~ 300 m) are used.

Maria Zatko 9/3/15 12:44 PM
Deleted: temperature-dependent

Maria Zatko 9/4/15 1:55 PM
Deleted: ,

Maria Zatko 9/4/15 1:55 PM
Deleted: E10, and

Maria Zatko 9/3/15 12:45 PM
Deleted: *T*

Maria Zatko 9/8/15 11:49 AM
Deleted:

Maria Zatko 10/13/15 10:03 AM
Deleted:

Maria Zatko 9/3/15 12:50 PM
Deleted: . ... [6]

Maria Zatko 9/8/15 11:43 AM
Deleted:

2.1.2 Calculating Radiative Transfer in Snow

A 2-stream, plane parallel snowpack actinic flux parameterization based on a 4-stream radiative transfer model [*Grenfell*, 1991] was developed and described in detail in Zatko et al. [2013] and has been implemented into GEOS-Chem for the purposes of this study. The parameterization is simple, broadly applicable, and allows for variation in snow and sky properties (e.g., solar zenith angle, cloud fraction) over time. Ice grains are assumed to be spherical in shape and light-absorbing impurities (LAI), including black carbon, brown carbon, dust, and organics, are assumed to be homogeneously distributed throughout the snow and always external to the ice grain. The snowpack actinic flux parameterization is used to calculate the UV actinic flux (photons cm^{-2} s^{-1} nm^{-1}) and the mean austral summer (DJF) e-folding depths (cm) across Antarctica (Figure 3a), which are both needed to calculate F_{NOx}. The snowpack actinic flux parameterization is most sensitive to radiation equivalent mean ice grain radii (r_e) and insoluble LAI in snow [*Zatko et al*., 2013]; higher concentrations of LAI in the snow and smaller r_e lead to shallower e-folding depths (z_e). Field and satellite measurements suggest significant increases in surface r_e throughout austral summer in Antarctica [*Jin et al*., 2008, *Klein*, 2014]. The r_e and snow density values used in this study are from observations reported in Gallet et al. [2011] and Klein [2014] and range from 86-360 μm and 260-360 kg m^{-3}, respectively. The mean Dome C vertical r_e profile from Gallet et al. [2011] is applied across Antarctica for all seasons except austral summer. During austral summer, larger surface r_e values are incorporated across all of Antarctica to simulate the rapid surface r_e growth reported in Klein [2014].

The concentration of black carbon (BC) in the model (Figure 3b) is calculated by scaling observed BC concentrations (C_{BC}) at Vostok [*Grenfell et al*., 1994] by the modeled annual average snow accumulation rates (kg m^{-2} yr^{-1}) from GEOS-Chem. However, high accumulation rates in coastal regions (700 kg m^{-2} yr^{-1}) lead to unrealistically low C_{BC}. The minimum C_{BC} values used in the model are 0.08 ng g^{-1}, which is comparable to the C_{BC} values measured in high snow accumulation rate regions in Antarctica, such as in the East Antarctic sea ice zone (0.1 ng g^{-1}) [*Bisiaux et al.,* 2012, *Zatko and Warren*, 2015]. Insoluble non-black carbon species (nonBC) including dust, brown carbon, and organics, are responsible for the majority (up to 89% at λ=305 nm) of the absorption of radiation at UV wavelengths [*Zatko et al*., 2013] in snow. These nonBC species and their concentrations have not been well quantified in snow. Based on observations reported in Zatko et al. [2013], we scale UV-absorption by insoluble nonBC to the absorption by insoluble black carbon in snow by assuming that at λ=650-700 nm, which is a wavelength range where black carbon dominates absorption, insoluble black carbon is responsible for 70% of the particulate absorption. We also assume that nonBC material has an absorption Ångstrom exponent of 5 [*Doherty et al*., 2010].

We neglect the influence of soluble light absorbers in the snow and only consider the influence of insoluble LAI on calculations of actinic flux profiles in snow. To determine whether soluble LAI contribute significantly to light-absorption in the snow, we calculate the total extinction coefficient for insoluble BC, insoluble nonBC, and soluble LAI following section 2.1 of Zatko et al. [2013] and using the absorption coefficients for

Maria Zatko 9/4/15 1:56 PM
Deleted: (Figure 3a)

Maria Zatko 9/4/15 1:58 PM
Deleted:

Maria Zatko 9/4/15 1:56 PM
Deleted: (Figure 3b)

Maria Zatko 9/4/15 1:59 PM
Deleted: , which show good agreement with observations (Figure 2a).

soluble material in snow reported in Beine et al., [2011] in northern Alaska. To our knowledge, observations of soluble light-absorbing impurities in Antarctic snow are unavailable. We use soluble LAI observations from the Arctic to provide a general estimate of the importance of soluble LAI in polar snow. The absorption coefficients (0.028 m^{-1} at λ=307 nm) from Beine et al. [2011] are identical to the extinction coefficients because it is assumed that there is no scattering by soluble species. Insoluble C_{BC} (9 ng g^{-1}) from Barrow, Alaska [*Doherty et al.*, 2010] were used to calculate extinction coefficients for BC and nonBC material and therefore the amount of nonBC absorption in the UV and near-visible wavelengths following Zatko et al. [2013]. Insoluble nonBC material is responsible for 9-14 times more absorption than soluble material in the wavelength range λ=298-345 nm. Insoluble BC material is responsible for 1.5-10 times more absorption than soluble material in the wavelength range λ=298-345 nm. The extinction coefficient is not influenced by the addition of a soluble absorber because scattering by snow grains dominates the extinction in snow. The effective co-albedo of single scattering is increased by 6-15% when soluble absorbers are included. The resulting change in z_e is at most 0.5 cm, which represents an increase of 4-9% in the wavelength region of λ=298-345 nm.

2.1.3. Calculating NO_3^- Concentrations in Snow

The median value of sub-surface (varied depth resolution) snow NO_3^- concentrations from the ITASE campaign (60 ng g^{-1}) [*Bertler et al.*, 2005] is used for modeled sub-surface (from 2-cm depth to the depth of the snow photic zone, z_{3e}) snow NO_3^- concentrations ($[NO_3^-]_{bot}$) across all of Antarctica. Although there is a large variation in snow NO_3^- concentrations from observations collected during the ITASE campaign (Figure 3d), there is no clear spatial pattern. Since NO_3^- concentrations in the top 2 cm of snow are up to 10 times higher than NO_3^- concentrations below 2-cm depth, the NO_3^- concentrations in the top 2 cm of snow ($[NO_3^-]_{top}$) are calculated by enhancing $[NO_3^-]_{bot}$ by a factor of 6, the median of observed NO_3^- enhancement factors (*EF*) in the top 2 cm of snowpack [*Dibb et al.*, 2004, *Erbland et al.*, 2013, *Frey et al.*, 2009, *Mayewski and Legrand*, 1990, *Rothlisberger et al.*, 2000]. Since NO_3^- concentrations are enhanced by a factor of 6 in the top 2 cm of snow, an equal amount of NO_3^- has been removed from the remainder of the photic-zone depth to maintain mass balance of nitrate within the snow column.

As mentioned in the introduction, the measured quantum yields for the dominant NO_3^- photolysis pathway (E1) range from 0.003 molec $photon^{-1}$ [*Chu and Anastasio*, 2003] to 0.6 molec $photon^{-1}$ [*Zhu et al.*, 2010] at T=253K. A higher fraction of NO_3^- was likely present on ice surfaces in the Zhu et al. [2010] study compared to the Chu and Anastasio [2003] study due to the different sample preparation methods, and likely explains the 3 order-of-magnitude difference in quantum yields. This interpretation suggests NO_3^- on the surface of ice grains is much more photolabile compared to NO_3^- embedded within ice grains, consistent with results from Meusinger et al. [2014]. In this study, we assume that NO_3^- that is wet deposited to the snow surface is more likely to be embedded in the interior of a snow grain compared to NO_3^- that is dry deposited to the surface of the snow grain, which is a simplistic scheme designed to take nitrate recombination chemistry into account. To simulate this effect in an idealized snowpack, we scale snow NO_3^- concentrations by the fraction of dry deposition relative to total (wet + dry) deposition to

Maria Zatko 9/11/15 10:16 AM
Deleted: Although there is a large variation in snow NO_3^- concentrations from observations collected during the ITASE campaign (Figure 3d), there is no clear spatial pattern, likely from the redistribution of NO_3^- resulting from photolysis and subsequent recycling.

Maria Zatko 9/11/15 9:27 AM
Deleted: below 2 cm

Maria Zatko 9/11/15 10:12 AM
Deleted:

Maria Zatko 9/10/15 6:33 PM
Deleted: below this depth

Maria Zatko 9/8/15 2:12 PM
Deleted: $1.3x10^{-3}$

Maria Zatko 10/14/15 2:22 PM
Deleted: account for

the Antarctic snow surface, assuming that only the fraction of dry deposited NO_3^- is photolabile (F_p). The degree of migration of NO_3^- within a snow grain after deposition due to snow metamorphism is unknown, which may influence the photolability of NO_3^- [*Domine and Shepson*, 2002]. Snow NO_3^- concentrations scaled by F_p are shown in Figure 3d.

Other modeling studies have attempted to calculate the fraction of photolabile NO_3^- in snow by estimating the concentration of NO_3^- contained within the liquid-like region (LLR) on the surface of ice grains (e.g., *Thomas et al.*, 2012). In this work, we do not explicitly calculate NO_3^- photolysis within the LLR because there are still many unknowns about the LLR [*Domine et al.*, 2013], including the distribution of NO_3^- between the bulk snow and the LLR. This distribution is better understood for some species, such as chloride [*Cho et al.*, 2002], but it is unclear if NO_3^- behaves similarly. In this study, we have assumed that all NO_x formed in the LLR is transferred to the boundary layer, which may lead to overestimates in the modeled F_{NOx} values presented in this study. The quantum yield for NO_3^- photolysis is dependent on the location of NO_3^- in snow, and although there are uncertainties surrounding the location of NO_3^- in snow, in this study we use the full range of measured quantum yields to provide bounds for the amount of NO_x produced from snow NO_3^- photolysis.

2.2. Model Sensitivity Studies

Due to uncertainties in our understanding of snow photochemistry [*Domine et al.*, 2013], we perform a variety of model sensitivity studies, as shown in Table 3. The quantum yield is varied from 0.002 molec photon^{-1} (corresponding to T=244 K) [*Chu and Anastasio*, 2003] to 0.6 molec photon^{-1} [*Zhu et al.*, 2010]. Snow NO_3^- concentrations below 2 cm ($[NO_3^-]_{bot}$) are halved and doubled with respect to the base case scenario and the impact of scaling NO_3^- concentrations by the fraction of photolabile NO_3^- (F_p) is investigated. The NO_3^- enhancement factor in the top 2 cm of snowpack is varied from 1 to 10, based upon a range of reported observations [*Dibb et al.*, 2004, *Frey et al.*, 2009, *Mayewski and Legrand*, 1990, *Rothlisberger et al.*, 2000]. C_{BC} is halved and doubled with respect to the base case scenario. The r_e profiles are varied in three sensitivity studies to examine the influence of r_e on the model-calculated mean austral summer (DJF) flux of snow-sourced NO_x ($\overline{F_{NOx}}$). The bulk extinction coefficient for snow ($Kext_{tot}$) is increased and decreased by 20% with respect to the base case scenario because Libois et al. [2013] suggest that the spherical snow grain assumption overestimates e-folding depths by a factor of 1.2. These sensitivity studies are used to provide estimates of the influence of these parameters on $\overline{F_{NOx}}$ throughout the Antarctic continent.

2.3. Estimating the Impact of Snow NO_3^- Photolysis on Boundary Layer Chemistry and Ice-Core NO_3^- Records

Nitrate photolysis, followed by oxidation, recycling, and redistribution of snow-sourced NO_x, influences both boundary layer chemistry and the concentration and isotopic signature of NO_3^- that is ultimately preserved in ice-core records. The preservation of NO_3^- in ice cores is most dependent on the amount of NO_3^- lost from the snow through photolysis via transport of snow-sourced NO_x away from the site of primary deposition.

Maria Zatko 9/4/15 2:06 PM
Deleted: (Figure 3c)

Maria Zatko 10/14/15 2:01 PM
Deleted:

Maria Zatko 10/14/15 5:12 PM
Deleted: 2

Maria Zatko 9/8/15 2:29 PM
Deleted: $1.3x10^{-3}$

Maria Zatko 9/12/15 8:30 AM
Deleted: preservation of

The methods used to explore and quantify nitrogen recycling and photolysis-driven loss of NO_3^- in snow are described in the following sections.

2.3.1. Reactive Nitrogen Recycling Between the Air and Snow

The Nitrogen Recycling Factor (*NRF*) is a metric originally proposed by Davis et al. [2008] to quantify the degree of reactive nitrogen recycling in snow over 1 year. The *NRF* is calculated in E8:

$$NRF = \frac{F_{NOx}}{F_{PRI}}, \quad \text{E8}$$

In E8, F_{NOx} (ng N m^{-2} yr^{-1}) is the annual sum of NO_x released from the snow and F_{PRI} (ng N m^{-2} yr^{-1}) is the annual sum of primary NO_3^- deposited to the snow. Davis et al. [2008] use the *NRF* to describe nitrogen recycling on both macro-scale (e.g., across the East Antarctic plateau) and micro-scale (e.g., the number of times one molecule of NO_3^- is recycled) levels. An *NRF* greater than 1 suggests that multiple nitrogen recycling events occur in the snow. *NRF* represents the average, or "bulk" degree of nitrogen recycling in snow because this global modeling study cannot resolve the degree of nitrogen recycling on a molecular level in the snow; some NO_3^- molecules may never be photolyzed while other NO_3^- molecules may be photolyzed and recycled many times greater than *NRF*. The *NRF* has implications for boundary layer chemistry because the continual re-emission of NO_x enhances the effective concentration of NO_x in the boundary layer [*Davis et al.*, 2008]. Additionally, nitrogen recycling between the air and snow may alter the preservation of NO_3^- in ice-core records.

2.3.2. Export of Snow-sourced Nitrate Away from the Original Site of Photolysis

Once snow-sourced NO_x is emitted to the atmosphere, it is subject to transport away from the original site of photolysis. If snow-sourced NO_x is oxidized to HNO_3 and re-deposited back to the snow surface, then there is no net photolysis-driven loss of NO_3^- from the snow. However, if some of the snow-sourced NO_x is transported away from the site of primary deposition, there is a net photolysis-driven loss of NO_3^- from the snow. The fraction of total NO_3^- (photolabile + non-photolabile) lost from the snow driven by photolysis (*f*) is calculated in E9:

$$f = \left(\left(\frac{F_R}{F_{NOx}}\right)^{\tau_z} - 1\right) \cdot F_p \quad \text{E9}$$

In E9, negative values of *f* represent loss of NO_3^- from the snow and positive values of *f* represent gain of NO_3^- to the snow. In E9, F_R (ng N m^{-2} yr^{-1}) is the total annual flux of recycled NO_3^- to the snow surface and F_{NOx} (ng N m^{-2} yr^{-1}) is the total annual flux of NO_x released from the snow. F_R is calculated by subtracting the depositional flux of NO_3^- from a model run without snow photochemistry from the depositional flux of NO_3^- from a model run with snow photochemistry. The ratio of F_R to F_{NOx} represents the fraction of photolabile NO_3^- remaining in the snow after 1 year. As long as NO_3^- remains in the photic zone, NO_3^- can continually be lost from the snow by photolysis-driven processes. The preservation of NO_3^- in ice cores is dependent on the fraction of NO_3^- lost from the snow through photolysis during the entire time that NO_3^- remains in the photic zone.

Maria Zatko 9/3/15 1:00 PM
Deleted: r

Maria Zatko 9/3/15 12:57 PM
Deleted: .

Maria Zatko 9/3/15 1:15 PM
Deleted: Similar to the NRF_{yr} in E9, NRF_{τ_z} values greater than 1 suggest that multiple nitrogen recycling events are occurring in the snow before burial beneath the photic zone.

Maria Zatko 9/3/15 1:30 PM
Deleted: We calculate the number of years that NO_3^- remains in the photic zone (τ_z, years) according to E9, where both the depth of the photic zone (cm) and the total annual snow accumulation (α_r) (cm yr^{-1}) are consid... [7]

Maria Zatko 9/3/15 1:34 PM
Deleted: 10

Maria Zatko 10/13/15 9:01 AM
Deleted: 1 –

Maria Zatko 9/3/15 1:34 PM
Deleted: 10

Maria Zatko 9/3/15 1:34 PM
Deleted: 10

Provided that there are no major changes in parameters that influence snow photochemistry (e.g., LAI, overhead ozone abundance) from year to year, the fraction of photolabile NO_3^- lost from the snow over 1 year will be stable from year to year.

τ_z (E10) represents the number of years that NO_3^- remains in the photic zone (τ_z, years) and in E9, τ_z accounts for the loss of NO_3^- that occurs during the entire time that it remains in the photic zone. When NO_3^- remains in the photic zone for less than a year (τ_z < 1), τ_z in E9 is set equal to 1. τ_z is calculated according to E10, where both the depth of the photic zone (cm) and the total annual snow accumulation (α_r) (cm yr^{-1}) are considered.

$$\tau_z = \frac{z_e}{\alpha_r}, \qquad \text{E10}$$

In E10, z_e (cm) is 1 e-folding depth of UV actinic flux and is used instead of z_{3e} because 87-91% of snow-sourced NO_x is produced within the top 1 e-folding depth. To convert total annual snow accumulation rate from kg m^{-2} yr^{-1} to cm, a typical snow density for Antarctica (0.36 g cm^{-3}) [*Grenfell et al.*, 1994] is assumed. τ_z is the minimum number of years on average that NO_3^- remains in the top one-third of the snow photic zone before burial beneath because nitrogen recycling, which effectively redistributes NO_3^- upwards in the snow, is not factored into E10. τ_z thus represents the lifetime of NO_3^- in snow in an average sense and does not resolve photolysis and recycling of individual NO_3^- molecules.

In E9, $\left(\left(\frac{F_R}{F_{NOx}}\right)^{\tau_z} - 1\right)$ represents the fraction of photolabile NO_3^- lost from the snow through photolysis. This fraction is multiplied by F_p to calculate the fraction of total (photolabile + non-photolabile) NO_3^- lost from the snow through photolysis (f). If f is 0, then all snow-sourced NO_x is redeposited to the snow and there is no net loss of NO_3^-. f is also 0 if the net export of snow-sourced NO_x away from the site of original photolysis is balanced by net import of snow-sourced NO_x from other Antarctic locations. If f is between -1 and 0, the export of local snow-sourced NO_x is higher than the deposition of snow-sourced NO_x from elsewhere in Antarctica, resulting in net photolysis-driven loss of NO_3^- from the snow. If f is greater than 0, the export of local snow-sourced NO_x is lower than the deposition of snow-sourced NO_x from elsewhere in Antarctica, resulting in net photolysis-driven gain of NO_3^- to the snow.

f is used to calculate the enrichment in ice-core $\delta^{15}N(NO_3^-)$ due solely to the impact of photolysis-driven loss of NO_3^- in snow. We use a Rayleigh fractionation equation used to calculate $\delta^{15}N(NO_3^-)$ [*Blunier et al.*, 2005]:

$$\delta^{15}N(NO_3^-) = \delta^{15}N(NO_3^-)_{air} \cdot (1 + f)^{\epsilon} - 1 \qquad \text{E11}$$

In E11, $\delta^{15}N(NO_3^-)_{air}$ is the annual-averaged $\delta^{15}N$ value of boundary layer NO_3^- and ε is the fractionation constant (-47.9‰ [*Berhanu et al.*, 2014]). In this work, we set $\delta^{15}N(NO_3^-)_{air}$ equal to 0‰ to investigate the enrichment in $\delta^{15}N(NO_3^-)$ only from photolysis-driven loss of NO_3^- from snow.

Maria Zatko 10/15/15 10:52 AM
Deleted: (E10)

Maria Zatko 9/3/15 1:32 PM
Moved (insertion) [1]

Maria Zatko 9/3/15 1:32 PM
Deleted: in E10

Maria Zatko 9/3/15 1:32 PM
Moved up [1]: τ_z in E10 accounts for the loss of NO_3^- that occurs during the entire time that it remains in the photic zone.

Maria Zatko 9/3/15 1:33 PM
Deleted: When NO_3^- remains in the photic zone for less than a year (τ_z < 1), τ_z in E10 is set equal to 1.

Maria Zatko 9/3/15 1:36 PM
Deleted: 10

Maria Zatko 10/13/15 9:08 AM
Deleted: 1 –

Maria Zatko 10/13/15 9:10 AM
Deleted: 0

Maria Zatko 10/13/15 9:10 AM
Deleted: 1

Maria Zatko 10/13/15 9:10 AM
Deleted: less

Maria Zatko 10/13/15 9:04 AM
Deleted: –

3. Results and Discussion

3.1. Parameters that Influence F_{NOX} and its Spatial Redistribution

Figure 2a shows modeled total annual snow accumulation rates from GEOS-Chem (kg m^{-2} yr^{-1}) along with estimated total annual snow accumulation rates (kg m^{-2} yr^{-1}) in Antarctica [*Erbland et al*., 2013, *Fegyveresi et al., 2011, Grenfell et al*., 1994], ranging from 10-700 kg m^{-2} yr^{-1}. The rapid decrease in snow accumulation rate from the coast to the top of the East Antarctic plateau is attributed to increased distance from the ocean (moisture source) and increased elevation. Figure 2b shows modeled annual mean surface wind divergence from May 2009 to May 2010. Figure 2b and Antarctic Mesoscale Prediction System surface wind output [Figure 3 in *Parish and Bromwich*, 2007] indicate that the large-scale airflow pattern in Antarctica flows from the East Antarctic plateau downslope towards the coast. There are three major regions of wind convergence in Antarctica, located near the Ross, Ronne, and Amery ice shelves.

Figure 3a shows the mean austral summer (DJF) e-folding depth of UV actinic flux in snow (z_e). z_e ranges from 24 to 69 cm, with the shallowest depths on the East Antarctic plateau, due to the relatively high C_{BC} values (Figure 3b). Higher C_{BC} in snow results in a shallower z_e because UV absorption in snow is enhanced as the concentration of LAI increases [*Zatko et al*., 2013]. In this study, coastal grid boxes are a mixture of water, sea ice, and snow-covered surfaces, and since actinic flux profiles are only calculated for snow-covered surfaces, the average z_e in coastal grid boxes are artificially shallow. Observations of e-folding depths across Antarctica are limited. France et al. [2011] report z_e from near-station snow at Dome C ranging from 9-20 cm at 350 nm, which agree well with our modeled z_e [*Zatko et al*., 2013]. There are no z_e observations in Antarctica from snow without station contamination, which is representative of the majority of snow in Antarctica. Zatko et al. [2013] calculate z_e of 38 cm (λ=298-345 nm) for remote Dome C snow due to lower C_{BC} far away from station contamination. The z_e for remote Dome C snow in this study (48 cm) is a factor of 1.3 larger than reported in Zatko et al. [2013] because larger radiation equivalent ice grain radii (r_e) are used during austral summer (based on Klein [2014]), and larger r_e grains lead to deeper z_e.

Figure 3b shows snow C_{BC}, ranging from 0.08 to 0.6 ng g^{-1}. Black carbon observations at WAIS-Divide [*Bisiaux et al*. 2012], Siple Dome [*Chylek et al*., 1992], Vostok [*Grenfell et al*., 1994], South Pole [*Warren and Clarke*, 1990], and Dome C [*Warren et al*., 2006] are included in Figure 3b. The highest C_{BC} values in Antarctica are found on the East Antarctic plateau (0.6 ng g^{-1}) and the spatial pattern of C_{BC} is governed by the snow accumulation rate; higher snow accumulation rates dilute C_{BC} [*Doherty et al*., 2013]. The modeled boundary layer black carbon concentrations are relatively uniform across Antarctica (0.1-0.6 pptv) because the majority of black carbon reaches Antarctica through long-range transport (with the exception of local production from Antarctic research stations).

Figure 3c shows the fraction of dry-deposited NO_3^- compared to total deposited NO_3^- across Antarctica. The ratio of dry deposition to total deposition ranges from 0 to 0.2 in coastal Antarctica and from 0.95 to 0.99 on the East Antarctic plateau. Figure 3d shows

Maria Zatko 10/14/15 4:11 PM
Deleted: , *Sofen et al*., 2014

Maria Zatko 9/4/15 2:14 PM
Deleted: There is good agreement between the modeled total snow accumulation rates in GEOS-Chem and previously reported total annual snow accumulation rates.

Maria Zatko 9/4/15 2:15 PM
Deleted: ,

Maria Zatko 9/4/15 2:16 PM
Deleted: which is in general agreement with

Maria Zatko 9/4/15 2:16 PM
Deleted: from

Maria Zatko 9/4/15 2:18 PM
Deleted: *Figure 3 in*

Maria Zatko 9/4/15 2:18 PM
Deleted: [

Maria Zatko 9/4/15 2:17 PM
Deleted: . The annual mean surface wind patterns

Maria Zatko 10/13/15 10:17 AM
Deleted: inaveraged over ,

Maria Zatko 10/15/15 10:52 AM
Deleted: Byrd

the modeled annual mean sub-surface (from 2-cm depth to the bottom of the photic zone, z_{3e}) snow NO_3^- concentrations ($[NO_3^-]_{bot}$=60 ng g^{-1}) scaled by F_p compared to averaged multi-year NO_3^- observations from the ITASE campaign [*Bertler et al.*, 2005] and mean asymptotic (sub-photic zone) NO_3^- mixing ratios from Erbland et al. [2013] and Shi et al. [2014].

3.2. Model Sensitivity Studies

Table 3 shows the dependence of mean austral summer (DJF) $\overline{F_{NOx}}$ on ϕ, $[NO_3^-]_{bot}$, C_{BC}, F_p, $Kext_{tot}$, r_e. The sensitivity study results are compared to $\overline{F_{NOx}}$ from the base case scenario, which is also described in Table 3. $\overline{F_{NOx}}$ is most sensitive to ϕ, which increases $\overline{F_{NOx}}$ by up to a factor of 330 compared to the base case scenario. The second most influential parameter is the concentration of photolabile NO_3^- ($[NO_3^-]_{bot}$ and F_p). Assuming that all NO_3^- is photolabile (F_p=1) increases $\overline{F_{NOx}}$ by up to a factor of 7.4 (at the coasts) with respect to the base case scenario. Variations in r_e, $Kext_{tot}$, EF, and C_{BC} influence $\overline{F_{NOx}}$ by up to a factor of 1.3 compared to the base case scenario. Appendix A shows model-calculated mean austral summer (DJF) $\overline{F_{NOx}}$ throughout Antarctica for the sensitivity studies described in Table 3. The quantum yield for NO_3^- photolysis and the concentration of photolabile NO_3^- are likely related to one another. This highlights the need for field, laboratory, and modeling studies to investigate factors influencing these parameters, such as the location of NO_3^- in ice grains.

Figure 4 shows model-calculated mean austral summer (DJF) $\overline{F_{NOx}}$ for several sensitivity studies compared to previously reported F_{NOx} at Neumayer [*Jones et al.*, 2001], Halley [*Bauguitte et al.*, 2012, *Jones et al.*, 2011], South Pole [*Oncley et al.*, 2004, *Wang et al.*, 2008, *Zatko et al.*, 2013], Dome C [*Frey et al.*, 2013, *Zatko et al.*, 2013], and WAIS-Divide [*Masclin et al.*, 2013]. The flux of snow-sourced NO_x is overestimated by three orders of magnitude compared to observations when ϕ from Zhu et al. [2010] is used to calculate $\overline{F_{NOx}}$. In contrast, model-calculated $\overline{F_{NOx}}$ using ϕ from Chu and Anastasio [2003] provides better agreement with the observations, but is lower than the observations by 14-78%. Use of the fraction of dry-deposited NO_3^- (F_p) to scale the concentration of photolabile NO_3^- lowers $\overline{F_{NOx}}$ by up to 85% along the coast, but has little impact on the East Antarctic plateau due to the high fraction of dry deposited NO_3^- (Figure 3c). The spatial patterns of $\overline{F_{NOx}}$ in Figure 4 are largely governed by the depth of the photic zone (z_e) across Antarctica (Figure 3a), which are inversely related to LAI concentrations. The spatial patterns of $\overline{F_{NOx}}$ are also influenced by the fraction of photolabile NO_3^-, which is lowest at the coast in the model.

Previously reported F_{NOx} values are calculated from measurements of NO_x concentration gradients and turbulent diffusivity [*Jones et al.*, 2001, 2011, *Frey et al.*, 2013] or calculated based on observed NO gradients and assuming photochemical steady-state [*Oncley et al.*, 2004], by incorporating observations into 1-D multi-phase chemistry models [*Bauguitte et al.*, 2012, *Boxe and Saiz-Lopez.*, 2008, *Wang et al.*, 2008], or by using depth-integrated F_{NOx} calculations similar to E7 [*France et al.*, 2011, *Masclin et al.*, 2013, *Zatko et al.*, 2013]. Observations of F_{NOx} represent either noontime maxima [*Bauguitte et al.*, 2012, *Frey et al.*, 2013, *Jones et al.*, 2001, *Zatko et al.*, 2013], daily averages [*Jones et al.*, 2011, *Masclin et al.*, 2013], or averages over the duration of the

Maria Zatko 10/12/15 5:32 PM
Deleted: average

Maria Zatko 9/10/15 6:36 PM
Deleted: below 2 cm

Maria Zatko 10/12/15 5:19 PM
Deleted: (3.7-797 ppb)

Maria Zatko 10/12/15 5:11 PM
Deleted: .

Maria Zatko 10/16/15 5:59 PM
Deleted: ,

Maria Zatko 9/6/15 2:18 PM
Deleted: or

Maria Zatko 9/7/15 4:13 PM
Deleted: *Boxe et al.*, 2008

field campaign [*Oncley et al.*, 2004, *Wang et al.*, 2008] (see Table 4 in Masclin et al., [2013]). There is a wide range of reported $\overline{F_{NOx}}$ at many of these locations; 2.4-17x10^8 molec cm^{-2} s^{-1} at Dome C [*France et al.*, 2011, *Frey et al.*, 2013, *Zatko et al.*, 2013], 3.2-22x10^8 molec cm^{-2} s^{-1} at South Pole [*Oncley et al.*, 2004, *Wang et al.*, 2008, *Zatko et al.*, 2013], 2.4-12.6x10^8 molec cm^{-2} s^{-1} at Halley [*Bauguitte et al.*, 2012, *Jones et al.*, 2011], 2.1-3.3x10^8 molec cm^{-2} s^{-1} at Neumayer [*Jones et al.*, 2001], 42.5x10^8 molec cm^{-2} s^{-1} at WAIS-Divide [*Masclin et al.*, 2013].

Regardless of the time period that the F_{NOx} observations represent, all F_{NOx} values for each location are averaged together and presented in Figure 4c and Figure 4d. Unfortunately, the actinic flux parameterization used here [*Zatko et al.*, 2013] is unable to resolve $\overline{F_{NOx}}$ directly at the coast because coastal grid boxes are a mixture of ocean, sea ice, and land, which prevents direct comparison of $\overline{F_{NOx}}$ at Halley and Neumayer. Since the flux of snow-sourced NO_x is overestimated by three orders of magnitude compared to observations when the quantum yield from Zhu et al. [2010] is used, all following results (Figures 5-10) are calculated using the Chu and Anastasio [2003] quantum yield (ϕ=1.3x10^{-3}). Additionally, to approximate the potential spatial variability in the fraction of NO_3^- that is photolabile, we scale snow NO_3^- by F_p in Figures 5-10. Figure 4d shows the $\overline{F_{NOx}}$ values, ranging from 0.5-7.8x10^8 molec cm^{-2} s^{-1}, used in Figures 5-10. All the other parameters used to calculate $\overline{F_{NOx}}$ in following sections and in Figures 5-10 are described in the base-case scenario in Table 3.

3.3. Redistribution and Recycling of Reactive Nitrogen Across Antarctica

Figure 5a shows the total annual depositional flux of primary NO_3^- (F_{PRI}), which ranges from 0.9-35x10^5 ng N m^{-2} yr^{-1} and is highest at the coasts due to its relative proximity to NO_x-source regions in lower latitudes. An adjoint modeling study by Lee et al. [2014] suggests that boundary layer NO_3^- abundance in Antarctica is dominated by NO_3^- transport to Antarctica originating from NO_x emissions from 25-65°S during austral winter and by thermal decomposition of peroxyacyl nitrate (PAN) as it descends from the free troposphere in all other seasons. Figure 5b shows the total annual depositional flux of recycled NO_3^- (F_R), which ranges from 0.7-31x10^5 ng N m^{-2} yr^{-1} and is also highest at the coasts due to transport from the Antarctic interior by katabatic winds. F_{PRI} and F_R are comparable in magnitude to the total annual flux of snow-sourced NO_x to the atmosphere (F_{NOx}), which ranges from 2-23x10^5 ng N m^{-2} yr^{-1} (Figure 4d). Figure 5c shows that recycled nitrogen (F_R) is the dominant form of NO_3^- deposition across Antarctica, except along the coastline where it represents as little as 11% of the deposition flux, and is most important in regions of wind convergence such as the Ronne, Ross, and Amery ice shelves.

To further investigate the role that wind patterns have on the redistribution of NO_3^- across Antarctica, we alternately turn off the upward F_{NOx} in East Antarctica and in West Antarctica to examine the influence of each region on NO_3^- redistribution across Antarctica. Figure 6 compares F_R in these sensitivity studies to F_R in the base case scenario. The large reduction in F_R when F_{NOx} is separately turned off in East and West Antarctica demonstrates that little snow-sourced NO_3^- is transported between East and West Antarctica, likely due to the influence of the trans-Antarctic mountains on

Maria Zatko 9/4/15 2:49 PM
Deleted: and comparing the mean $\overline{F_{NOx}}$ observation at each site with modeled $\overline{F_{NOx}}$ values in this study allows for a coarse examination of the model-measurement agreement.

Maria Zatko 9/4/15 3:19 PM
Deleted: 3

Maria Zatko 9/12/15 12:26 PM
Deleted: xyacl

atmospheric transport. However, recycled NO_3^- is present in West Antarctica where F_{NOx} has been turned off, suggesting that some snow-sourced NO_3^- from East Antarctica is transported across the trans-Antarctic mountains likely due to the influence of katabatic winds originating from the East Antarctic plateau.

Figure 7 shows the Nitrogen Recycling Factor (*NRF*). Across Antarctica, *NRF* ranges from 0 to 16, indicating that nitrogen is recycled multiple times over the course of 1 year across most of Antarctica, with the exception of the coasts. The spatial pattern of *NRF* is governed by the flux of snow-sourced NO_x to the atmosphere ($\overline{F_{NOx}}$, Figure 4d), which is influenced by the depth of the photic zone (z_e) and the concentration of photolabile nitrate. The spatial pattern of *NRF* is also dependent on F_{PRI}, which is highest at the coast and lowest on the East Antarctica plateau. *NRF* values are lowest near the coast because the fraction of photolabile NO_3^- is small and F_{PRI} values are high. The maximum *NRF* values occur partway up the plateau, corresponding to maximum $\overline{F_{NOx}}$ values. Erbland et al. [2015] use a multi-layer snow chemistry column model along with snow and atmospheric NO_3^- concentration and isotopic measurements to estimate the *NRF* at Dome C. The difference in model-estimates of nitrogen recycling at Dome C in Erbland et al. [2015] (4 recycling events) and in this study (9 recycling events) is at least partially due to the assumption in Erbland et al. that 20% of snow-sourced NO_3^- is transported away from Dome C via katabatic winds. We use our global chemical transport modeling framework to calculate that 25% of snow-sourced NO_3^- is transported away at Dome C, which is slightly larger than the assumption in Erbland et al. [2015]. Larger NO_3^- export fractions will lead to larger loss of snow nitrate, which may also lead to a larger number of recycling events via transport and redeposition of snow-sourced NO_x throughout East Antarctica. Davis et al. [2008] use estimates of atmospheric NO_x overhead-column burdens and average NO_x atmospheric lifetimes along with primary nitrogen deposition measurements from Legrand and Kirchner [1990] to estimate the *NRF* in East Antarctica. Davis et al. [2008] estimate an *NRF* of 1.8, which is roughly 3 to 6 times lower than the modeled East Antarctic *NRF* values in this study (*NRF*=5-10), although Davis et al. state that their estimated *NRF* value could be factors of 3 to 5 times higher due to uncertainties in primary nitrogen deposition estimates.

3.4. Impact of Reactive Nitrogen Recycling on Boundary Layer Chemistry

The height of the boundary layer will strongly influence the abundance of NO_3^-, reactive nitrogen oxides, and oxidants emitted or formed at or near the surface. At many Antarctic stations (e.g., Neumayer, South Pole, Dome C, Halley, Kohnen) there is a wide range of observed boundary layer heights during austral summer (10-600 m [*Casasanta et al.*, 2014, *Davis et al.*, 2004, *Handorf*, 1996, *Jones et al.*, 2006, 2008, *King et al.*, 2006, *Kodama et al.*, 1985, *Konig-Langlo et al.*, 1998, *Neff et al.*, 2008, *Oncley et al.*, 2004, *Travouillon et al.*, 2008, *Weller et al.*, 1999]), and although modeled boundary layer heights are not systematically biased in one direction compared to observations, they often do not agree well. Therefore, only the relative impacts of snow photochemistry on reactive nitrogen and oxidant abundances are compared in this study. The impact of snow photochemistry on boundary layer chemistry can be examined by considering factor changes in boundary layer NO_x, NO_3^-, OH, and O_3 mixing ratios between simulations with and without snow NO_3^- photolysis. As shown in Figure 8, the inclusion of a snow

Maria Zatko 9/3/15 1:45 PM

Deleted: Figure 7b shows the minimum number of years that snow NO_3^- remains in the photic zone on average, τ_z (E9). Nitrate remains in photic zone for 3 months near the Antarctic coasts and up to 7.5 years on the East Antarctic plateau before burial below the photic zone. The spatial pattern of τ_z is governed by the snow accumulation rate, both directly and indirectly through its influence on C_{BC}. The spatial pattern of τ_z is in agreement with the expectation that NO_3^- remains in the photic zone the longest in areas with low snow accumulation rates.

NO_x source leads to factor increases in boundary layer mixing ratios of NO_x from 7.0-31.6, gas-plus aerosol-phase nitrate from 3.9-38.1, OH from 3.6-6.7, and O_3 from 1.3-2.0. The largest factor increases are in West Antarctica, particularly near the Ross and Ronne ice shelves, where winds carrying photo-produced species converge. The surface transport pattern is especially important for the redistribution of the longer-lived species NO_3^- and O_3. Other snow photochemical reactions mentioned in the introduction but not included in this modeling study will also impact oxidant abundances, but the effects of each photochemical reaction are not be additive due to the highly non-linear nature of oxidant cycling.

3.5. Implications for Ice-Core Records of Nitrate Concentrations and Isotopes

Figure 9a shows the minimum number of years that snow NO_3^- remains in the photic zone on average, τ_z (E9). NO_3^- remains in photic zone for 3 months near the Antarctic coasts and up to 7.5 years on the East Antarctic plateau before burial below the photic zone. The spatial pattern of τ_z is governed by the snow accumulation rate, both directly and indirectly through its influence on C_{BC}. The spatial pattern of τ_z is in agreement with the expectation that NO_3^- remains in the photic zone the longest in areas with low snow accumulation rates.

Figure 9b shows the fraction of NO_3^- gained or lost from the snow through photolysis (f, E11), which ranges from -0.99 to 0.21. The positive f values indicate regions with net gain of NO_3^- to the snow resulting from the spatial redistribution of NO_3^- driven by snow photochemistry. In regions of convergence, such as over the Ronne Ice Shelf, and parts of the coast, there is a net gain of snow-sourced NO_3^-. There is a sharp gradient in f between the plateau and the coast, with the largest loss of snow NO_3^- on the East Antarctic plateau. On the East Antarctic plateau, most photolyzed NO_3^- is transported away by katabatic winds, but along the coast, the photolysis-driven loss of NO_3^- from the snow is minimal due to high snow accumulation rates and transport of snow-sourced NO_3^- from the continental interior. The spatial pattern of f is largely influenced by the number of years that NO_3^- remains in the photolytic zone (τ_z), the concentration of photolabile NO_3^- (F_p), and wind patterns across Antarctica.

Figure 9c shows modeled enrichments in ice-core $\delta^{15}N(NO_3^-)$ from photolysis-driven loss of NO_3^- in snow, compared to sub-photic zone $\delta^{15}N(NO_3^-)$ observations from Erbland et al. [2013], Frey et al. [2009], Jarvis, [2008], Shi et al., [2014], and Sofen et al. [2014]. The $\delta^{15}N(NO_3^-)$ values at Dome C and along the transect from Dumont d'Urville to Dome C are calculated asymptotic $\delta^{15}N(NO_3^-)$ values from Erbland et al. [2013] and Frey et al. [2009], which are representative of snow depths well below the photic zone at Dome C. The $\delta^{15}N(NO_3^-)$ values along the transect from Dome A towards Zhongshan are asymptotic $\delta^{15}N(NO_3^-)$ values calculated in Shi et al. [2014]. The $\delta^{15}N(NO_3^-)$ values at WAIS-Divide [*Sofen et al.*, 2014] and South Pole [*Jarvis*, 2008] are average ice-core $\delta^{15}N(NO_3^-)$ measurements from 1900-2000 CE, which are also representative of $\delta^{15}N(NO_3^-)$ values well below the snow photic zone. Model-calculated ice-core $\delta^{15}N(NO_3^-)$ values range from 0‰ to 363‰. The modeled enrichments in ice-core $\delta^{15}N(NO_3^-)$ values are generally higher than the sub-photic zone $\delta^{15}N(NO_3^-)$ observations presented in Figure 9c, however, boundary layer $\delta^{15}N(NO_3^-)$ observations are negative in

Maria Zatko 9/3/15 1:46 PM
Deleted: a

Maria Zatko 9/12/15 5:37 PM
Deleted: lost

Maria Zatko 10/13/15 9:12 AM
Deleted: 21

Maria Zatko 10/13/15 9:12 AM
Deleted: 99

Maria Zatko 10/13/15 9:12 AM
Deleted: negative

Maria Zatko 9/3/15 1:46 PM
Deleted: b

Maria Zatko 9/11/15 4:49 PM
Deleted: over much of Antarctica

both coastal [*Morin et al.*, 2009, *Savarino et al.*, 2007, *Wagenbach et al.*, 1998] and continental [*Erbland et al.*, 2013, *Frey et al.*, 2009] Antarctica, making modeled $\delta^{15}N(NO_3^-)$ values biased high by up to ~40‰ since we assume that the $\delta^{15}N$ of atmospheric nitrate (NO_3^- and HNO_3) deposited to the snow surface is always equal to 0‰. The modeled ice-core $\delta^{15}N(NO_3^-)$ values resulting from the photolysis-driven loss of snow nitrate are sensitive to the fractionation constant (ε). The fractionation constant is varied over the full range of values reported in Erbland et al [2013], Frey et al., [2009], and Shi et al. [2014]; an ε of –90‰ increases modeled ice-core $\delta^{15}N(NO_3^-)$ by a factor of 2 and an ε of -10‰ decreases modeled ice-core $\delta^{15}N(NO_3^-)$ by a factor of 5 across Antarctica. Both the modeled and observed $\delta^{15}N(NO_3^-)$ values show that $\delta^{15}N(NO_3^-)$ is most enriched on the East Antarctic plateau, where the fraction of NO_3^- lost from the snow through photolysis is highest.

3.6. Relationship Between Nitrogen Recycling and Photolytic-loss of NO_3^- in Snow

The degree of photolysis-driven loss of snow NO_3^- is determined by both rates of photolysis and transport patterns across the Antarctic continent. The spatial patterns of recycling (*NRF*, Figure 7) and loss (*f*, Figure 9b) differ across Antarctica and Figure 10 shows the relationship between *f* and *NRF* across Antarctica. The magnitude of nitrogen recycling and degree of photolysis-driven loss of snow NO_3^- are well correlated ($r^2 > 0.8$, $p < 0.001$) in regions where NO_3^- remains in the photic zone for less than 3 years ($\tau_z < 3$) (Figure 10a). The relationship between recycling and loss breaks down in locations where NO_3^- remains in the photic zone for more than 3 years (Figure 10b). The relationship between recycling and loss weakens with increasing τ_z because recycling of reactive nitrogen occurs at or near the surface only, while loss of NO_3^- occurs throughout the depth of snow photic zone. The number of years that NO_3^- remains in the snow photic zone (τ_z, E10) is mainly dependent on snow accumulation rates and the concentrations of light-absorbing impurities in snow, which are partially governed by snow accumulation rates. In the present climate, τ_z less than 3 years corresponds to snow accumulation rates higher than 85 kg m^{-2} a^{-1}.

4. Conclusions

We have incorporated the photolysis of snow NO_3^- into a global chemical transport model (GEOS-Chem) for the first time in order to calculate the flux and redistribution of nitrogen in Antarctic snowpack. An important goal of this study is to investigate the impact of snowpack NO_3^- photolysis on boundary layer chemistry and the preservation of NO_3^- concentration and isotopes in Antarctic ice cores.

The calculated flux of snow-sourced NO_x from Antarctic snow (0.5-7.8x10^8 molec cm^2 s^{-1}) is in general agreement with snow NO_x-flux observations when using a quantum yield for snow NO_3^- photolysis on the order of 10^{-3} molec $photon^{-1}$ [*Chu and Anastasio*, 2003]. The flux of snow-sourced NO_x is overestimated by 2-3 orders of magnitude when the quantum yield from Zhu et al. [2010] is used along with various assumptions for the amount of photolabile NO_3^-. The modeled spatial pattern of the flux of snow-sourced NO_x is determined by the patterns of light-absorbing impurity concentrations in snow and the fraction of photolabile NO_3^- across Antarctica. In the model, the spatial pattern of light-absorbing impurities is strongly influenced by snow accumulation rates and the

Maria Zatko 9/11/15 4:43 PM
Formatted: Font:Italic

Maria Zatko 9/11/15 4:45 PM
Deleted: [*Erbland et al.*, 2013, *Frey et al.*, 2009, *Morin et al.*, 2009, *Savarino et al.*, 2007],

Maria Zatko 9/11/15 4:42 PM
Deleted: 0

Maria Zatko 10/13/15 12:19 PM
Deleted: .

Maria Zatko 9/14/15 5:36 PM
Formatted: Left

Maria Zatko 9/11/15 6:34 PM
Deleted: snow accumulation rate and

Maria Zatko 9/11/15 6:38 PM
Deleted: aerosol

Maria Zatko 9/14/15 5:33 PM
Deleted:

spatial pattern of photolabile NO_3^- in the model is influenced by the amount of wet deposited NO_3^- compared to total deposited NO_3^- across Antarctica. Total snow NO_3^- concentrations were kept spatially constant in this study; however, spatial variations in snow NO_3^- concentrations would also influence the spatial pattern of F_{NOx} across Antarctica. However, observations of snow NO_3^- concentrations across Antarctica show no clear spatial pattern. Snow-sourced NO_x is subject to transport across Antarctica, and recycled NO_3^- makes up a large fraction of the depositional NO_3^- flux across the Antarctic continent, especially in regions of convergence over the Ronne, Ross, and Amery ice shelves.

The inclusion of snow-sourced NO_x in GEOS-Chem leads to factor increases in boundary layer mixing ratios for NO_x ranging from 7.0-31.6, gas and aerosol phase nitrate ranging from 3.9-38.1, OH ranging from 3.6-6.7, and O_3 ranging from 1.3-2.0. The incorporation of additional snow photochemical reactions into GEOS-Chem will also impact oxidant abundances, but the effects of each photochemical reaction are not be additive due to the highly non-linear nature of oxidant cycling.

The Nitrogen Recycling Factor (*NRF*) ranges from 0.07 to 15.8, suggesting that nitrogen is recycled multiple times on average over the course of one year across all of Antarctica, except at the coasts where snow accumulation rates are high. Nitrate can remain in the photic zone for up to 7.5 years in Antarctic snow and is recycled multiple times (up to 57, on average) before burial beneath the photic zone in Antarctica. The fraction of NO_3^- lost from the snow through photolysis ranges from -0.99 to 0.21, where negative values indicate net loss of NO_3^- from the snow. Photolysis of snow NO_3^- results in a net gain of NO_3^- in parts of West Antarctica, such as near the Ronne Ice Shelf where winds converge. The fraction of NO_3^- lost from the snow through photolysis is highest on the East Antarctic plateau (up to -0.99). The fraction of NO_3^- lost from the snow through photolysis is used to calculate the enrichment in ice-core $\delta^{15}N(NO_3^-)$ solely from photolysis-driven NO_3^- loss in snow. The modeled enrichment in ice-core $\delta^{15}N(NO_3^-)$ ranges from 0‰ to 363‰ and are in agreement with the broad-scale spatial patterns of observed sub-photic zone $\delta^{15}N(NO_3^-)$ observations. A significant relationship exists between nitrogen recycling and photolysis-driven loss of snow NO_3^- when NO_3^- remains in the photic zone for less than 3 years ($\tau_z < 3$), corresponding to a snow accumulation rate greater than 85 kg m^{-2} a^{-1} in the present day. Since the spatial variability of Antarctic ice-core $\delta^{15}N(NO_3^-)$ is mainly determined by the fractional loss of snow NO_3^-, observations of $\delta^{15}N(NO_3^-)$ in snow and ice can be used to estimate both the degree of recycling and loss of snow NO_3^- in Antarctica as long as this condition is met. The relationship between recycling and loss can be useful for the interpretation of the oxygen isotopic composition of ice-core NO_3^- (e.g., Sofen et al. [2014]). We note that the relationship between τ_z and snow accumulation rate may vary in different climates depending on the concentrations of light-absorbing impurities in snow [*Geng et al.*, 2015].

This is the first modeling study to incorporate snow NO_3^- photolysis into a global chemical transport model to investigate the impacts of a snow-NO_x source on boundary layer chemistry and nitrogen recycling and redistribution across Antarctica. Model results

Maria Zatko 9/11/15 6:37 PM
Deleted: .

Maria Zatko 10/12/15 12:33 PM
Deleted: downward

Maria Zatko 10/12/15 12:33 PM
Deleted: yr

Maria Zatko 9/12/15 7:48 AM
Deleted: Along the Antarctic coast, the NRF_{τ_z} is less than 1, which suggests that ice-core NO_3^- is relatively well preserved in coastal regions.

Maria Zatko 10/13/15 9:14 AM
Deleted: -0.21

Maria Zatko 10/13/15 9:14 AM
Deleted: 99

Maria Zatko 10/13/15 9:15 AM
Deleted: gain

Maria Zatko 10/13/15 9:15 AM
Deleted: to

Maria Zatko 10/15/15 10:55 AM
Deleted: with the magnitude

Maria Zatko 10/15/15 10:55 AM
Deleted: and

Maria Zatko 10/15/15 10:55 AM
Deleted: The agreement between observed and modeled $\delta^{15}N(NO_3^-)$ suggests that its spatial variability across the Antarctic continent is determined by the degree of photolysis-driven loss of snow NO_3^-.

Maria Zatko 10/14/15 1:06 PM
Deleted: The variability in the spatial patterns of nitrogen recycling and photolysis-driven NO_3^- loss in snow are broadly consistent across much of Antarctica, suggesting that ice-core $\delta^{15}N(NO_3^-)$ measurements can be used to examine the degree of nitrogen recycling in addition to NO_3^- loss in most of Antarctica.

shown here are broadly consistent with observations of the flux of NO_x from the Antarctic snowpack and snow $\delta^{15}N(NO_3^-)$, suggesting that the model captures the large-scale features of nitrogen recycling and loss across the Antarctic continent. Model sensitivity studies suggest that the flux of snow-sourced NO_x and loss of snow NO_3^- is most sensitive to the quantum yield for NO_3^- photolysis and the concentration of photolabile NO_3^-, which are likely related to one another. We suggest that future field, laboratory, and modeling studies continue to focus on gaining a better understanding of the quantum yield for NO_3^- photolysis and the concentration of photolabile NO_3^-. Updated information about the quantum yield for NO_3^- photolysis and the concentration of photolabile NO_3^- in snow along with additional snow photochemical reactions can be incorporated into this modeling framework in the future, which will continue to improve our understanding of the impacts of snow photochemistry on boundary layer chemistry and the preservation of NO_3^- and other photochemically-active species in ice cores.

Maria Zatko 10/15/15 10:56 AM
Deleted: impuritie

Acknowledgments

We acknowledge support from NSF PLR 1244817, NSF PLR 0944537, NSF PLR 1446904, and an EPA STAR graduate fellowship to M.C. Zatko. The authors thank Steve Warren, Sarah Doherty, Thomas Grenfell, and Quentin Libois for helpful discussions about light-absorbing impurities in snow and their influence on snow photochemistry. We thank Joseph Erbland for many helpful comments and discussions about nitrogen recycling. Joel Thornton and Lyatt Jaeglé also provided many helpful comments about this work. We also thank Paul Hezel and Yanxu Zhang for helping M.C. Zatko learn GEOS-Chem. Lastly, we thank Qianjie Chen for helpful feedback on paper drafts and Martin Schneebeli for providing useful advice about snow grain profiles in Antarctic snow.

References

Allen, D., Pickering, K., Duncan, B., Damon, M.: Impact of lightning NO emissions on North American photochemistry as determined using the Global Modeling Initiative (GMI) model. *J. Geophys. Res*., 115, D22301, doi:10.1029/2010JD014062, 2010.

Alexander, B., Savarino, J., Kreutz, K.J., Thiemens, M.H.: Impact of preindustrial biomass burning emissions on the oxidation pathways of tropospheric sulphur and nitrogen. *J. Geophys. Res.*, 109, D08303, doi:10.1029/2003/JD004218, 2004.

Amos, H. M., Jacob, D.J, Holmes, C.D, Fisher, J.A, Wang, Q., Yantosca, R.M., Corbitt, E.S., Galarneau, E., Rutter, A.P., Gustin, M.S., Steffen, A., Schauer, J.J, Graydon, J.A., St. Louis, V.L., Talbot, R.W., Edgerton, E.S., Zhang, Y., Sunderland, E.M.: Gas-Particle Partitioning of Atmospheric Hg(II) and Its Effect on Global Mercury Deposition, *Atmos. Chem. Phys.*, **12**, 591-603, 2012.

Anastasio, C., Galbavy, E. S., Hutterli, M. A., Burkhart, J. F., Friel, D. K.: Photoformation of hydroxyl radical on snow grains at Summit, Greenland. Atmos. Environ., 41, 5110-5121, doi:10.1016/j.atmosenv.2006.12.011, 2007.

Anastasio, C. and Chu, L.: Photochemistry of nitrous acid (HONO) and nitrous acidium ion (H_2ONO^+) in aqueous solution and ice. *Environ. Sci. Tech*., 43, 1108-1114, 2009.

Bauguitte, S.J.-B., Bloss, W.J., Evans, M.J., Salmon, R.A., Anderson, P.S., Jones, A.E., Lee, J.D., Saiz-Lopez, A., Roscoe, H.K., Wolff, E.W., Plane, J.M.C.: Summertime NOx measurements during the CHABLIS campaign: can source and sink estimates unravel observed diurnal cycles? *Atmos. Chem. Phys*., 12, 989-1002, doi:10.5194/acp-12-989-2012, 2012.

Beine, H., Anastastio, C., Esposito, G., Patten, K., Wilkening, E., Domine, F., Voisin, D., Barret, M., Houdier, S., Hall, S.: Soluble, light-absorbing species in snow at Barrow, Alaska. *J. Geophys. Res*., 116, D00R05, doi: 10.1029/2011JD016181, 2011.

Berhanu, T. A., Meusinger, C., Erbland, J., Jost, R., Bhattcharya, S. K., Johnson, M. S., Savarino, J.: Laboratory study of nitrate photolysis in Antarctic snow. II. Isotopic effects and wavelength dependence. J. Chem. Phys., 140, 244306, doi:10.1063/1.4882899, 2014.

Bertler, N., Mayewski, P. A., Aristarain, A., Barrett, P., Becagli, S., Bernardo, R., Bo, S., Xiao, C., Curran, M., Qin, D., Dixon, D., Ferron, F., Fischer, H., Frey, M., Frezzotti, M., Fundel, F., Genthon, C., Gragnani, R., Hamilton, G., Handley, M., Hong, S., Isaksson, E., Kang, J., Ren, J., Kamiyama, K., Kanamori, S., Karkas, E., Karlof, L., Kaspari, S., Kreutz, K., Kurbatov, A., Meyerson, E., Ming, Y., Zhang, M., Motoyama, H., Mulvaney, R., Oerter, H., Osterberg, E., Proposito, M., Pyne, A., Ruth, U., Simoes, J., Smith, B., Sneed, S., Teinila, K., Traufetter, F., Udisti, R., Virkkula, A., Watanabe, O., Williamson, R., Winther, J-G., Li, Y., Wolff, E., Li, Z., Zielinski, A.: Snow chemistry across Antarctica, *Annals of Glaciology*, *41*(1), 167- 179, 2005.

Bey, I., Jacob, D.J., Yantosca, R.M., Logan, J.A., Field, B.D., Fiore, A.M., Li, Q., Liu, H.Y., Mickley, L.J., Schultz, M.G.: Global modeling of tropospheric chemistry with assimilated meteorology: Model description and evaluation, *J. Geophys. Res.*, *106*(D19), 23073-23095, 2001.

Bian, H.S., Prather, M.J.: Fast-J2: Accurate simulation of stratospheric photolysis in global chemical models. *J. Atmos. Chem*., 41, 281-296, 2002.

Bisaux, M. M., Edwards, R., McConnell, J. R., Curran, M. A. J., Van Ommen, T. D., Smith, A. M., Neumann, T. A., Pasteris, D. R., Penner, J. E., Taylor, K.: Changes in black carbon deposition to Antarctica from two high-resolution ice core records, 1850-2000 AD. *Atmos. Chem. Phys*., 12, 4107-4115, doi: 10.5194/acp-12-4107-2012, 2012.

Bloss, W.J., Lee, J.D., Heard, D.E., Salmon, R.A., Bauguitte, S.J-B., Roscoe, H.K., Jones, A.E.: Observations of OH and HO_2 radicals in coastal Antarctica. Atmos. Chem. Phys., 7, 4171-4185, 2007.

Boxe, C.S., Colussi, A.J., Hoffmann, M.R., Murphy, J.G., Wolldridge, P.J., Bertram, T.H., Cohen, R.C.: Photochemical production and release of gaseous NO_2 from nitrate-doped water ice. J. Phys. Chem., A, 109, 8520-8525, 2005.

Boxe, C.S., Saiz-Lopez, A.: Multiphase modeling of nitrate photochemistry in the quasi-liquid layer (QLL): implications for NOx release from the Arctic and coastal Antarctic snowpack. *Atmos. Chem. Phys*., 8, 4855-4864, 2008.

Blunier, T., Gregoire, F. L., Jacobi, H.-W., and Quansah, E.: Isotopic view on nitrate loss in Antarctic surface snow. *Geophys. Res. Lett*., 32, L13501, doi:10.1029/2005GL023011, 2005.

Casasanta, G., Pietroni, I., Petenko, I., Argentini, S.: Observed and modelled convective mixing-layer height in Dome C, Antarctica. *Boundary-Layer Meteorol.*, 151, 597-608, doi:10.1007/s10546-014-9907-5, 2014.

Chen, G., Davis, D., Crawford, J., Hutterli, L.M., Huey, L.G., Slusher, D., Mauldin, L., Eisele, F., Tanner, D., Dibb, J., Buhr, M., McConnell, J., Lefer, B., Shetter, R., Blake, D., Song, C.H., Lombardi, K., Arnoldy, J.: A reassessment of HO_x South Pole chemistry based on observations recorded during ISCAT 2000. *Atmos. Environ*., 38, 5451-5461, 2004.

Chu, L., and Anastasio. C.: Quantum Yields of Hydroxyl Radicals and Nitrogen Dioxide from the Photolysis of Nitrate on Ice. *J. Phys. Chem. A*., 107, 9594-9602, 2003.

Cho, H., Shepson, P.B., Barrie, L.A., Cowin, J.P., Zaveri, R.: NMR Investigation of the Quasi-Brine Layer in Ice/Brine Mixtures. *J. Phys. Chem. B*., 106, 11226-11232, 2002.

Chylek, P., Johnson, B., Wu, H.: Black carbon concentration in Byrd station ice core – From 13,000 to 700 years before present. Ann. Geophys., 10, 625-629, 1992.

Davis, D., Chen, G., Buhr, M., Crawford, J., Lenschow, D., Lefer, B., Shetter, R., Eisele, F., Mauldin, L., Hogan, A.: South Pole NOx Chemistry: an assessment of factors controlling variability and absolute levels. *Atmos. Environ*., 38, 5375-5388, 2004.

Davis, D. D., Seelig, J., Huey, G., Crawford, J., Chen, G., Wang, Y., Buhr, M., Helmig, D., Neff, W., Blake, D., Arimoto, R., Eisele, F.: A reassessment of Antarctic plateau reactive nitrogen based on ANTCI 2003 airborne and ground based measurements. *Atmos. Environ*., 42, 2831-2848, doi:10.1016/j.atmosenv.2007.07.039, 2008.

Dibb, J. E., Huey, G. L., Slusher, D. L., and Tanner, D. J.: Soluble reactive nitrogen oxides at South Pole during ISCAT 2000. *Atmos. Environ*., 38, 5399-5409, 2004.

Doherty, S. J., Warren, S. G., Grenfell, T. C., Clarke, A. D., and Brandt, R. E.: Light-absorbing impurities in Arctic snow. *Atmos. Chem. Phys*., 10, 11647-11680, doi:10.5194/acp-10-11647-2010, 2010.

Doherty, S. J., Grenfell, T.C., Forsstrom, S., Hegg, D.L., Brandt, R.E., Warren, S.G.: Observed vertical redistribution of black carbon and other insoluble light-absorbing particles in melting snow, *J. Geophys. Res. Atmos.*, 118, 1-17, doi:10.1002/jgrd.50235, 2013.

Domine, F., Shepson, P. B.: Air-snow interactions and atmospheric chemistry, *Science*, 297, 1506–1510, 2002.

Domine, F., Bock, J., Voisin, D., Donaldson, D. J.: Can we model snow photochemistry? Problems with the current approaches. *J. Phys. Chem. A*, 117, 4733-4749, doi: 10.1021/jp3123314 2013.

Erbland, J., Vicars, W.C., Savarino, J., Morin, S., Frey, M.M., Frosini, D., Vince, E., Martins, J.M.F.: Air-snow transfer of nitrate on the East Antarctic Plateau – Part 1: Isotopic evidence for a photolytically driven dynamic equilibrium in summer. *Atmos. Chem. Phys.*, 13, 6403-6419, doi:10.5194/acp-13-6403-2013, 2013.

Erbland, J., Savarino, J., Morin, S., France, J.L., Frey, M.M., King, M.D.: Air-snow transfer of nitrate on the East Antarctic plateau – Part 2: An isotopic model for the interpretation of deep ice-core records. *Atmos. Chem. Phys. Discuss.*, 15,6886-6966, doi:10.5194/acpd-15-6887-2015, 2015.

Fegyveresi, J.M., Alley, R.B., Spencer, M.K., Fitzpatrick, J.J., Steig, E.J., White, J.W.C., McConnell, J.R., Taylor, K.C.: Late-Holocene climate evolution at the WAIS Divide site, West Antarctica: bubble number-density estimates. J. *Glaciol.*, 57, 204, 2011.

Fisher, J.A., Jacob, D.J., Wang, Q., Bahreini, R., Carouge, C.C., Cubison, M.J., Dibb, J.E., Diehl, T., Jimenez, J.L., Leibensperger, E.M., Meinders, M.B.T., Pye, H.O.T., Quinn, P.K., Sharma, S., van Donkelaar, A., Yantosca, R.M.: Sources, distribution, and acidity of sulfate-ammonium aerosol in the Arctic in winter-spring, *Atmos. Environ.*, 45, 7301-7318, 2011.

France, J.L., King, M.D., Frey, M.M., Erbland, J., Picard, G., Preunkert, S., MacArthur, A., Savarino, J.: Snow optical properties at Dome C (Concordia), Antarctica; implications for snow emissions and snow chemistry of reactive nitrogen. *Atmos. Chem. Phys.*, 11, 9787-9801, doi:10.5194/acp-11-9787-2011, 2011.

Frey, M. M., Savarino, J., Morin, S., Erbland, J., and Martins, J. M. F.: Photolysis imprint in the nitrate stable isotope signal in snow and atmosphere of East Antarctica and implications for reactive nitrogen cycling. *Atmos. Chem. Phys.*, 9, 8681-8696, 2009.

Frey, M. M., Brough, N., France, J. L., Anderson, P.S., Traulle, O., King, M.D., Jones, A.E., Wolff, E.W., Savarino, J.: The diurnal variability of atmospheric nitrogen oxides (NO and NO_2) above the Antarctic Plateau driven by atmospheric stability and snow emissions. *Atmos. Chem. Phys.*, 13, 3045-3062, doi:10.5194/acp-13-3045-2013, 2013.

Freyer, H. D., Kley, D., Voiz-Thomas, A., Kobel, K.: On the interaction of isotopic exchange processes with photochemical reactions in atmospheric oxides of nitrogen. *J. Geophys. Res. Atmos.*, 98(D8), 14791-14796, 1993.

Gallet, J.-C., Domine, F., Arnaud, L., Picard, G., and Savarino, J.: Vertical profiles of the specific surface area and density of the snow at Dome C and on a transect to Dumont D'Urville, Antarctica – albedo calculations and comparison to remote sensing products. The Cryosphere., 5, 631-649, doi: 10.5194/tc-5-631-2011, 2011.

Geng, L., Alexander, B., Cole-Dai, J., Steig, E.J., Savarino, J., Sofen, E.D., Schauer, A.J.: Nitrogen isotopes in ice core nitrate linked to anthropogenic atmospheric acidity change. *Proc. Natl. Acad. Sci*., 111, 16, 5808-5812, doi:10.1073/pnas.1319441111, 2014a.

Geng, L., Cole-Dai, J., Alexander, B., Erbland, J., Savarino, J., Schauer, A. J., Steig, E.J., Lin, P., Fu, Q., Zatko, M.C.: On the origin of the occasional springtime nitrate concentration maximum in Greenland. Snow. Atmos. Chem. Phys., 14, 13361-13376, doi:10.5194/acp-14-13361-2014, 2014b.

Geng, L., Zatko, M.C., Alexander, B., Fudge, T.J., Schauer, A.J., Murray, L.T., Mickley, L.J.: Effects of post-depositional processing on nitrogen isotopes of nitrate in the Greenland Ice Sheet Project 2 (GISP2) ice core. *Geophys. Res. Lett*., doi:10.1002/2015GL064218, 2015.

Grannas, A. M., Jones, A. E., Dibb, J., Ammann, M., Anastasio, C., Beine, H. J., Bergin, M., Bottenheim, J., Boxe, C. S., Carver, G., Chen, G., Crawford, J. H., Domine, F., Frey, M. M., Guzman, M. I., Heard, D. E., Helmig, D., Hoffman, M. R., Honrath, R. E., Huey, L. G., Hutterli, M., Jacobi, H. W., Klan, P., Lefer, B., McConnell, J., Plane, J., Sander, R., Savarino, J., Shepson, P. B., Simpson, W. R., Sodeau, J. R., von Glasow, R., Weller, R., Wolff, E. W., Zhu, T.: An overview of snow photochemistry: evidence, mechanisms and impacts. *Atmos. Chem. Phys*., 7, 4329-4373, 2007.

Grenfell, T. C.: A Radiative Transfer Model for Sea Ice With Vertical Structure Variations. *J. Geophys. Res*., 96, 16991-17001, 1991.

Grenfell, T.C., Warren, S.G, Mullen, P.C.: Reflection of solar radiation by the Antarctic snow surface at ultraviolet, visible, and near-infrared wavelengths. *J. Geophys. Res*., 99, 18669-18684, 1994.

Handorf, D., Foken, T., Kottmeier, C.: The stable atmospheric boundary layer over an Antarctic ice sheet. *Boundary-Layer Meteorol*, 91, 165-189, 1999.

Hastings, M.G., Sigman, D.M., Steig, E.J.: Glacial/interglacial changes in the isotopes of nitrate from the Greenland Ice Sheet Project (GISP2) ice core. *Global Biogeochem. Cycles*, 19:GB4024, doi:10.1029/2005GB002502, 2005.

Heaton, T. H. E., Spiro, B., Robertson, M. C. S.: Potential canopy influences on the isotopic composition of nitrogen and sulphur in atmospheric deposition. *Oecologia*, 109, 4, 600-607, 1997.

Helmig, D., Johnson, B., Oltmans, S.J., Neff, W., Eisele, F., Davis, D.: Elevated ozone in the boundary layer at South Pole. *Atmos. Environ*., 42, 2788-2803, 2008.

Holtslag, A.A.M., Boville, B.: Local versus nonlocal boundary layer diffusion in a global climate model. *J. Clim*., 6, 1825–1842, 1993.

Hudman, R.C., N.E. Moore, R.V. Martin, A.R. Russell, A.K. Mebust, L.C. Valin, and R.C. Cohen, A mechanistic model of global soil nitric oxide emissions: implementation and space based-constraints, *Atmos. Chem. Phys*., 12, 7779-7795, doi:10.5194/acp-12-7779-2012, 2012.

Jarvis, J. C.: Isotopic studies of ice core nitrate and atmospheric nitrogen oxides in polar regions. Ph.D. Thesis, University of Washington, publication number 3328411, 2008.

Jin, Z., Charlock, T.P., Yang, P., Xie, Y., Miller, W.: Snow optical properties for different particle shapes with application to snow grain size retrieval and MODIS/CERES radiance comparison over Antarctica. *Remote. Sens. Environ*., 112, 3563-3581, 2008.

Jones, A., Weller, R., Anderson, P., Jacobi, H., Wolff, E., Schrems, O., Miller, H.: Measurements of NO_x emissions from the Antarctic snowpack. *Geophys. Res. Lett*., 28, 1499-1502, doi: 10.1029/2000GL011956, 2001.

Jones, A.E., Anderson, P.S., Wolff, E.W., Turner, J., Rankin, A.M., Colwell, S.R.: A role for newly forming sea ice in springtime polar tropospheric ozone loss? Observational evidence from Halley station, Antarctica. *J. Geophys. Res*., 111, D08306, doi:10.1029/2005JD006566, 2006.

Jones, A.E., Wolff, E.W., Salmon, R.A., Bauguitte, S.J.-B., Roscoe, H.K., Anderson, P.S., Ames, D., Clemitshaw, K.C., Fleming, Z.L., Bloss, W.J., Heard, D.E., Lee, J.D., Read, A.K., Hamer, P., Shallcrossm, D.E., Jackson, A.V., Walker, S.L., Lewis, A.C., Mills, G.P., Plane, J.M.C., Saiz-Lopez, A., Sturges, W.T., Worton, D.R.: Chemistry of the Antarctic Boundary Layer and the Interface with Snow: an overview of the CHABLIS campaign. *Atmos. Chem. Phys*., 8, 3789-3803, 2008.

Jones, A.E., Wolff, E.W., Ames, D., Bauguitte, S. J.-B., Clemitshaw, K.C., Fleming, Z., Mills, G.P., Saiz-Lopez, A., Salmon, R.A., Sturges, W.T., Worton, D.R.: The multi-seasonal NO_y budget in coastal Antarctica and its link with surface snow and ice core nitrate: results from the CHABLIS campaign. *Atmos. Chem. Phys*., 11, 9271-9285, doi:10.5194/acp-11-9271, 2011, 2011.

King, J.C., Argentini, S.A., Anderson, P.S.: Contrasts between the summertime surface energy balance and boundary layer structure at Dome C and Halley stations, Antarctica. *J. Geophys. Res*., 111, D02105, doi:10.1029/2005JD006130, 2006.

Klein, K.: Variability in dry Antarctic firn; Investigations on spatially distributed snow and firn samples from Dronning Maud Land, Antarctica. Ph.D. Thesis, Universitat Bremen. hdl: 10013/epic.44893. http://nbn-resolving.de/urn:nbn:de:gbv:46-00104117-15, date last access: April 15, 2014.

Kodama, Y., Wendler, G., Ishikawa, N.: The diurnal variation of the boundary layer in summer in Adelie Land, Eastern Antarctica. *J. Appl. Met*., 28, 16-24, 1989.

Konig-Langlo, G., King, J., Pettre, P., Climatology of the three coastal Antarctic stations Durmont D'urville, Neumayer, and Halley. *J. Geophys. Res*., D9, 103, 10935-10946, 1998.

Lee, H., Henze, D.K., Alexander, B., Murray, L.T.: Investigating the sensitivity of surface-level nitrate seasonality in Antarctica to primary sources using a global model. *Atmos. Environ*., 89, 757-767, doi:10.1016/j.atmosenv.2014.03.003, 2014.

Legrand, M.R., Kirchner, S.: Origins and variations of nitrate in South Polar precipitation. *J. Geophys. Res*., 95, 3493-3507, 1990.

Levy, H., Moxim, W.J., Klonecki, A.A., Kasibhatla, P.S.: Simulated tropospheric NOx: Its evaluation, global distribution and individual source contributions. *J. Geophys. Res*., 104, 26279-26306, 1999.

Libois, Q., Picard, G., France, J. L., Arnaud, L., Dumont, M., Carmagnola, C. M., King, M. D.: Grain shape influence on light extinction in snow. *The Cyrosphere*, 7, 1803-1818, doi:10.5194/tc-7-1803-2013, 2013.

Lin, S.J., Rood, R.B.: Multidimensional flux form semi-Lagrangian transport schemes. *Mon. Wea. Rev*., 124, 2046-2070, 1996.

Lin, J. T., McElroy, M.B.: Impacts of boundary layer mixing on pollutant vertical profiles in the lower troposphere: Implications to satellite remote sensing. *Atmos. Environ*., 44, 1726-1749, doi:10.1016/j.atmosenv.2010.02.009, 2010.

Liu, H., Jacob, D.J., Bey, I., Yantosca, R.M.: Constraints from ^{210}Pb and ^{7}Be on wet deposition and transport in a global three-dimensional chemical tracer model driven by assimilated meteorological fields, *J. Geophys. Res.*, *106*(D11), 12,109-112,128, 2001.

Logan, J.A., Nitrogen oxides in the troposphere: Global and regional budgets. *J. Geophys. Res*., 88(C15), 10785-10807, doi:10.1029/JC088iC15p10785, 1983.

Mack, J., and Bolton, J. R.: Photochemistry of nitrite and nitrate in aqueous solution: A review. *J. Photochem. Photobiol*. A., 128, 1-13, 1999.

Mao, J., Jacob, D.J., Evans, M.J., Olson, J.R., Ren, X., Brune, W.H., St. Clair, J.M., Crounse, J. D., Spencer, K.M., Beaver, M.R., Wennberg, P.O., Cubison, M.J., Jimenez, J.L., Fried, A., Weibring, P., Walega, J.G., Hall, S.R., Weinheimer, A.J., Cohen, R.C., Chen, G., Crawford, J.H., Jaegle, L., Fisher, J.A., Yantosca, R.M., Le Sager, P., Carouge, C.: Chemistry of hydrogen oxide radicals (HO_x) in the Arctic troposphere in spring. *Atmos. Chem. Phys*., 10, 5823-5838, doi:10.5194/acp-10-5823-2010, 2010.

Masclin, S., Frey, M. M., Rogge, W. F., Bales, R. C.: Atmospheric nitric oxide and ozone at the WAIS Divide deep coring site: a discussion of local sources and transport in West Antarctica. *Atmos. Chem. Phys*., 13, 8857-8877, doi:10.5194/acp-13-8857-2013, 2013.

Mayewski, P. A., and Legrand, M. R.: Recent increase in nitrate concentration of Antarctic snow. *Nature,* 346, 258-260, 1990.

Meusinger, C., Berhanu, T.A., Erbland, J., Savarino, J., Johnson, M.S.: Laboratory study of nitrate photolysis in Antarctic snow. I. Observed quantum yield, domain of photolysis, and secondary chemistry. *J. Chem. Phys*., 140, 244305, doi:10.1063/1.4882898, 2014.

Morin, S., Savarino, J., Frey, M.M., Domine, F., Jacobi, H.-W., Kaleschke, L., Martins, J.M.F.: Comprehensive isotopic composition of atmospheric nitrate in the Atlantic Ocean boundary layer from 65°S to 79°N. *J. Geophys. Res*., 114, D05303, doi:10.1029/208JD010696, 2009.

Mulvaney, R., Wagenbach, D., Wolff, E.W.: Postdepositional change in snowpack nitrate from observation of year-round near-surface snow in coastal Antarctica. *J. Geophys. Res*., 103, 11021-11031, 1998.

Murray, L.T., Jacob, D.J., Logan, J.A., Hudman, R.C., Koshak, W.J.: Optimized regional and interannual variability of lightning in a global chemical transport model constrained by LIS/OTD satellite data, *J. Geophys. Res*., 117, D20307, 2012.

Neff, W., Helmig, D., Grachev, A., Davis, D.: A study of boundary layer behaviour associated with high concentrations at the South Pole using a minisoder, tethered balloon, and a sonic anemometer. *Atmos. Environ*., 42, 2762-2779, doi:10.1029/2012JD017934, 2008.

Oliver, J.G.J., Van Aardenne, J.A., Dentener, F.J., Pagliari, V., Ganzeveld, L.N., Peters, J.A.H.W.: Recent trends in global greenhouse gas emissions: regional trends 1970-2000 and spatial distribution of key sources in 2000. Env. Sci., 2(2-3), 81-99, doi:10.1080/15693430500400345, 2005.

Oncley, S., Buhr, M., Lenschow, D., Davis, D., Semmer, S.: Observations of summertime NO fluxes and boundary-layer height at the South Pole during ISCAT 2000 using scalar similarity. *Atmos. Environ*., 38, 5389-5398, doi:10.1016/j.atmosevn.2004.05.053, 2004.

Parish, T. R., and D. H. Bromwich (2007), Reexamination of the near-surface airflow over the Antarctic continent and implications on atmospheric circulations at high southern latitudes, *Monthly Weather Review*, *135*, 1961-1973.

Parrella, J.P., Jacob, D.J., Liang, Q., Zhang, Y., Mickley, L.J., Miller, B., Evans, M.J., Yang, X., Pyle, J.A., Theys, N., Van Roozendael, M.: Tropospheric bromine chemistry: implications for present and pre-industrial ozone and mercury. *Atmos. Chem. Phys*., 12, 6723-6740, doi:10.5194/acp-12-6723-2012, 2012.

Pratt, K. A., Custard, K. D., Shepson, P. B., Douglas, T. A., Pohler, D., General, S., Zielcke, J., Simpson, W. R., Platt, U., Tanner, D. J., Huey, L. G., Carlsen, M., Stirm, B. H.: Photochemical production of molecular bromine in Arctic surface snowpacks. *Nature*, 6, 351-356, doi:10.1038/NGEO1779, 2013.

Price, C., Rind, D.: A simple lightning parameterization for calculating global lightning distributions. *J. Geophys. Res*., **97**, 9919–9933, 1992.

Rothlisberger, R., Hutterli, M. A., Sommer, S., Wolff, E. W., and Mulvaney, R.: Factors controlling nitrate in ice cores: Evidence from the Dome C deep ice core. J. Geophys. Res., 105, 20565-20572, 2000.

Sander, S. P., Friedl, R.R., Golden, D.M., Kurylo, M.J., Moortgat, G.K., Keller-Rudek, H., Wine, P.J., Ravishankara, A.R., Kolb, C.E., Molina, M.J., Finalyson-Pitts, B.J., Huie, R.E., Orkin, V.L.: Chemical kinetics and photochemical data for use in atmospheric studies evaluation number 15. JPL Publications, Pasadena, 1-523, 06-2, 2006.

Savarino, J., Kaiser, J., Morin, S., Sigman, D.M., Thiemens, M.H.: Nitrogen and oxygen isotopic constraints on the origin of atmospheric nitrate in coastal Antarctica. *Atmos. Chem. Phys*., 7, 1925-1945, 2007.

Simpson, W. R., von Glasow, R., Riedel, K., Anderson, P., Ariya, P., Bottenheim, J., Burrows, J., Carpenter, L. J., Friess, U., Goodsite, M. E., Heard, D., Hutterli, M., Jacobi, H.-W., Kaleschke, L., Neff, B., Plane, J., Platt, U., Richter, A., Roscoe, H., Sander, R., Shepson ,P., Sodeau, J., Steffen, A., Wagner, T., Wolff, E.: Halogens and their role in polar boundary-layer ozone depletion. *Atmos. Chem. Phys*., 7(16):4375–4418, 2007.

Slusher, D. L., Huey, L. G., Tanner, D. J., Chen, G., Davis, D. D., Buhr, M., Nowak, J. B., Eisele, F. L., Kosciuch, E., Mauldin, R. L., Lefer, B. L., Shetter, R. E., Dibb, J. E.: Measurements of pernitric acid at the South Pole during ISCAT 2000. *Geophys. Res. Lett*., 29, 21, doi:10.1029/2002GL015703, 2002.

Shi, G., Buffen, A.M., Hastings, M.G., Li, C., Ma, H., Li, Y., Sun, B., An, C., Jiang, S.: Investigation of post-depositional processing of nitrate in East Antarctica snow: isotopic constraints on photolytic loss, re-oxidation, and source inputs. *Atmos. Chem. Phys. Discuss*., 14, 31943-31986, doi: 10.5194/acpd-14-31943-2014, 2014.

Sjostedt, S.J., Huey, L.G., Tanner, D.J., Peischl, J., Chen, G., Dibb, J.E., Lefer, B., Hutterli, M.A., Beyersdorf, A.J., Blake, N.J., Blake, D.R., Sueper, D., Ryerson, T., Burkhart, J., Stohl, A.: Observations of hydroxul and the sum of peroxy radicals at Summit, Greenland during summer 2003. *Atmos. Environ*., 41, 5122-5137, 2007.

Sofen, E.D., Alexander, B., Steig, E.J., Thiemens, M.H., Kunasek, S.A., Amos, H.M., Schauer, A.J., Hastings, M.G., Bautista, J., Jackson, T.L., Vogel, L.E., McConnell, J.R., Pasteris, D.R., Saltzmann, E.S.: WAIS Divide ice core suggests sustained changes in the atmospheric formation pathways of sulfate and nitrate since the 19th century in the extratropical Southern Hemisphere. *Atmos. Chem. Phys*., 14, 5749-5769, doi:10.5194/acp-14-5749-2014, 2014.

Thomas, J. L., Dibb, J. E., Huey, L. G., Liao, J., Tanner, D., Lefer, B., von Glasow, R., Stutz, J.: Modeling chemistry in and above snow at Summit, Greenland – Part 2: Impact of snowpack chemistry on the oxidation capacity of the boundary layer. *Atmos. Chem. Phys*., 12, 6537-6554, doi:10.5194/acp-12-6537-2012, 2012.

Thompson, A.M., The oxidizing capacity of the Earth's atmosphere: Probable past and future changes. *Science*, 256, 1157-1165, 1992.

Travouillon, T., Ashley, M.C.B., Burton, M.G., Storey, J.W.V., Loewenstein, R.F.: Atmospheric turbulence at the South Pole and its implications for astronomy. *Astronom. And Astrophys*., 400, 1163-1172, doi:10.1051/0004-6361:20021814, 2003.

UNEP/WMO. Integrated Assessment of Black Carbon and Tropospheric Ozone: Summary for Decision Makers, UNON/Publishing Services Section/Nairobi, ISO 14001:2004, 2011.

van Donkelaar, A., R. V. Martin, W. R. Leaitch, A.M. Macdonald, T. W. Walker, D. G. Streets, Q. Zhang, E. J. Dunlea, J. L. Jimenez, J. E. Dibb, L. G. Huey, R. Weber, and M. O. Andreae. Analysis of Aircraft and Satellite Measurements from the Intercontinental Chemical Transport Experiment (INTEX-B) to Quantify Long-Range Transport of East Asian Sulfur to Canada. *Atmos. Chem. Phys*., **8**, 2999-3014, 2008.

van der Werf, G.R, Morton, D.C., DeFries, R.S., Giglio, L., Randerson, J.T., Collatz, G.J., Kasibhatla, P.S.: Estimates of fire emissions from an active deforestation region in the southern Amazon based on satellite data and biogeochemical modeling. *Biogeosciences*, **6** (2):235-249, 2009.

Wagenbach, D., Legrand, M., Fischer, H., Pichlmayer, F., Wolff, E.W.: Atmospheric near-surface nitrate at coastal Antarctic sites. *J. Geophys. Res*., 103, 11007-11020, 1998.

Wang, Y. H., Jacob, D.J., Logan, J.A.: Global simulation of tropospheric O3-NOx hydrocarbon chemistry 1. Model formulation, *J. Geophys. Res.*, *103*, 10,713-710,725, 1998.

Wang, Y., Choi, Y., Zeng, T., Davis, D., Buhr, M., Huey, G. L., and Neff, W.: Assessing the photochemical impact of snow NO_x emissions over Antarctica during ANTCI 2003. *Atmos. Environ*., 41, 3944-3958, doi:10.1016/j.atmosenv.2007.01.056, 2008.

Wang, Q., Jacob, D.J., Fisher, J.A., Mao, J., Leibensperger, E.M., Carouge, C.C., Le Sager, P., Kondo, Y., Jimenez, J. L., Cubison, M. J., Doherty, S.: Sources of carbonaceous aerosols and deposited black carbon in the Arctic in winter-spring: implications for radiative forcing. *Atmos. Chem. Phys*., 11, 12453-12473, doi:10.5194/acp-11-12453-2011, 2011.

Warren, S.G., Clarke, A.D.: Soot in the atmosphere and snow surface of Antarctica. *J. Geophys. Res*., 95, 1811-1816, 1990.

Warren, S. G., Brandt, R. E., and Grenfell, T. C.: Visible and near-ultraviolet absorption spectrum of ice from transmission of solar radiation into snow. *Appl. Opt*., 45, 5320-5334, 2006.

Weller, R., Minikin, A., Konig-Langlo, G., Schrems, O., Jones, A.E., Wolff, E.W., Anderson, P.S.: Investigating possible causes of the observed diurnal variability in Antarctica NO_y. *Geophys. Res. Lett*., 26, 18, 2853-2856, 1999.

Wesely, M. L.: Parameterization of surface resistances to gaseous dry deposition in regional-scale numerical-models, *Atmos. Env.*, *23*, 1293-130, 1989.

Wild, O., Q. Zhu, and M. J. Prather (2000), Fast-J: Accurate simulation of in- and below-cloud photolysis in global chemical models, *J. Atm. Chem.*, *37*, 245-282.

Wolff, E.W.: Nitrate in polar ice, in *Ice Core Studies of Global Biogeochem. Cycle*s, NATO ASI Ser., Ser. I, pp. 195-224, edited by R.J. Delmas, Springer, New York, 1995.

Wolff, E.W., Jones, A.E., Bauguitte, S. J.-B., Salmon, R.A.: The interpretation of spikes and trends in concentration of nitrate in polar ice cores, based on evidence from snow and atmospheric measurements. *Atmos. Chem. Phys*., 8, 5627-5634, 2008.

Xu, L., Penner, J.E.: Global simulations of nitrate and ammonium aerosols and their radiative effects. *Atmos. Chem. Phys*., 12, 9479-9504, doi:10.5194/ac[-12-9479-2012, 2012.

Zatko, M.C., Grenfell, T.C., Alexander, B., Doherty, S.J., Thomas, J.L., Yang, X., The influence of snow grain size and impurities on the vertical profiles of actinic flux and associated NO_X emissions on the Antarctic and Greenland ice sheets. *Atmos*. *Chem*. *Phys*., 13, 3547-3567, doi:10.5194/acp-13-3547-2013, 2013.

Zatko, M.C. and Warren, S.G.: East Antarctic sea ice in spring: spectral albedo of snow, nilas, frost flowers, and slush; and light-absorbing impurities in snow. *Ann. Glaciol.*

Special Issue: Sea ice in a changing environment, 56(69), 53-64, doi:10.3189/2015AoG69A574, 2015.

Zhang, L., S. Gong, J. Padro, and L. Barrie.: A size-segregated particle dry deposition scheme for an atmospheric aerosol module, *Atmos. Env.*, *35*, 549-560, 2001.

Zhu, C., Xiang, B., Chu, L.T., Zhu, L.: 308 nm Photolysis of Nitric Acid in the Gas Phase, on Aluminum Surfaces, and on Ice Films. *J. Phys. Chem. A*., 114, 2561-2568, doi: 10.1021/jp909867a, 2010.

Table 1. Glossary of variables used in this paper.

Variable	Unit	Description
λ	nm	Wavelength
ϕ	molec photon^{-1}	Quantum yield for NO_3^- photolysis
σ_{NO3^-}	cm^2	Absorption cross-section for NO_3^- photolysis
I	photons cm^{-2} s^{-1} nm^{-1}	Actinic flux of UV radiation
z_e	cm	e-folding depth of UV actinic flux in snow
z_{3e}	cm	Depth of snow photic zone
α_r	kg m^{-2} yr^{-1}	Total annual snow accumulation rate
C_{BC}	ng g^{-1}	Annual mean snow black carbon concentration
r_e	µm	Radiation equivalent mean ice grain radii
$Kext_{tot}$	cm^{-1}	Bulk extinction coefficient for snow
$[NO_3^-]_{top}$	ng g^{-1}	Mean NO_3^- concentration in top 2 cm of snow
$[NO_3^-]_{bot}$	ng g^{-1}	Mean NO_3^- concentration from 2-cm depth to the bottom of the snow photic zone
EF	unitless	NO_3^- enhancement factor in top 2 cm of snow
F_p	fraction	Fraction of photolabile NO_3^- in snow
$\Delta^{17}O(NO_3^-)$	‰	Oxygen isotopic composition of NO_3^-
$\delta^{15}N(NO_3^-)$	‰	Nitrogen isotopic composition of NO_3^-
ε	‰	Fractionation constant for NO_3^- photolysis
$\overline{F_{NOx}}$	molec cm^{-2} s^{-1}	Mean austral summer flux of snow-sourced NO_x
F_{NOx}	ng N m^{-2} yr^{-1}	Annual sum of snow-sourced NO_x flux
F_{PRI}	ng N m^{-2} yr^{-1}	Annual sum of primary NO_3^- deposited to snow
F_R	ng N m^{-2} yr^{-1}	Annual sum of recycled NO_3^- to snow
NRF_{yr}	unitless	Metric to assess degree of nitrogen recycling in 1 year
NRF_{τ_z}	unitless	Metric to assess degree of nitrogen recycling before NO_3^- burial below snow photic zone
τ_z	years	Years NO_3^- remains in snow photic zone
f	fraction	Fraction of photolysis-driven loss of NO_3^- from snow

Maria Zatko 9/10/15 6:41 PM
Deleted: in below 2 cm snow depth

Table 2. Value(s) of parameters used in the model.

Variable	Value(s) used in model	References
ϕ	0.002 molec photon^{-1}[a]	Chu and Anastasio [2003]
σ_{NO3^-}	2.7x10^{-20} cm^2 (λ=298-307 nm) 2.4x10^{-20} cm^2 (λ=307-312 nm) 1.9x10^{-20} cm^2 (λ=312-320 nm) 2.3x10^{-21} cm^2 (λ=320-345 nm)	Sander et al. [2006]
ε	-47.9‰	Berhanu et al. [2014]
r_e	Jan: 332.0 µm[b] Dec-Feb: 198-332.0 µm[b] Mar-Nov: 86.0-332.0 µm[b]	Gallet et al. [2011] Klein [2014]
ρ_{snow}	260-360 kg m^{-3}[c]	Gallet et al. [2011]
EF^b	6[d]	Dibb et al. [2004] Erbland et al. [2013] Frey et al. [2009] Mayewski and Legrand [1990] Rothlisberger et al. [2000]
$[NO_3^-]_{bot}$	60 ng g^{-1}[e]	Bertler et al. [2005]

[a] At temperature (T) = 244K

[b] r_e is varied vertically and temporally, but uniformly across Antarctica based on Gallet et al. [2011] and Klein [2014]. In January, r_e is constant with depth (332 µm), in December and February, r_e ranges from 198 µm at the snow surface to 332 µm at 300 cm depth, and from March to November, r_e ranges from 86 µm at the surface to 360 µm at 300 cm depth.

[c] The mean vertical ρ_{snow} profile from several Dome C snowpits are used in this study (see Figure 11 in Gallet et al. [2011]).

[d] Median of observed NO_3^- enhancement factors.

[e] Median of observed sub-surface snow NO_3^- mixing ratios from the ITASE campaign.

Table 3. Dependence of mean austral summer (DJF) flux of snow-sourced NO_x ($\overline{F_{NOx}}$) on quantum yield (ϕ), the fraction of photolabile NO_3^- (F_p), snow NO_3^- concentrations below 2 cm ($[NO_3^-]_{bot}$), the radiation equivalent ice grain radius (r_e), the bulk snow extinction coefficient ($Kext_{tot}$), the NO_3^- concentration enhancement factor in the top 2 cm (EF), and snow black carbon concentration (C_{BC}).

Parameter	Base case values[a]	Values used in sensitivity studies	$\overline{F_{NOx}}$ range in sensitivity studies ($\times 10^8$ molec cm^{-2} s^{-1})	Corresponding Figures
Quantum yield (ϕ)	0.002 molec photon^{-1} [b]	0.6 molec photon^{-1}	5-2600	Fig. 4a, b, c, d Fig. 1Aa
Fraction of photolabile NO_3^- (F_p)	0.01-0.99 (spatial variation, Figure 3c)	Set to 1 everywhere	3.7-9.6	Fig. 4c, d
Sub-surface snow NO_3^- ($[NO_3^-]_{bot}$)	60.0 ng g^{-1}[c]	30-120 ng g^{-1}	0.3-15.8	Fig. 1Ab, c
Radiation equivalent mean ice grain radii (r_e)	Jan: 332.0 μm[d] Dec-Feb: 198-332.0 μm[d] Mar-Nov: 86.0-332.0 μm[d]	Study 1: 332.0 μm[e] Study 2: 198-332.0 μm[e] Study 3: 86.0-332.0 μm[e]	0.5-10.2	Fig. 1Aj, k, l
Bulk snow extinction coefficient ($Kext_{tot}$)	1.7-6.9x10^3 m^{-1} (spatial variation)	± 20% with respect to base case values	0.5-9.4	Fig. 1Ah, i
NO_3^- enhancement factor in top 2 cm (EF)	6.0[f]	1-10	0.5-9.3	Fig. 1Af, g
Snow black carbon (C_{BC})	0.08-0.6 ng g^{-1} (spatial variation, Figure 3b)	± factor of 2 with respect to base case values	0.5-8.6	Fig. 1Ad, e

[a] base case F_{NOx}=0.5-7.8x10^8 molec cm^{-2} s^{-1} (Figure 4d)

[b] from Chu and Anastasio [2003] at T=244K

[c] median of ITASE campaign [*Bertler et al*., 2005]

[d] r_e is varied vertically and temporally, but uniformly across Antarctica based on Gallet et al. [2011] and Klein [2014]. In January, r_e is constant with depth (332 μm), in December and February, r_e ranges from 198 μm at the snow surface to 332 μm at 300 cm depth, and from March to November, r_e ranges from 86 μm at the surface to 360 μm at 300 cm depth.

[e] in r_e sensitivity study 1, the base-case 'January' r_e profile is applied for every month. In r_e sensitivity study 2, the base-case 'December and February' r_e profile is applied for every month. In r_e sensitivity study 3, the base-case 'March-November' r_e profile is applied for every month.

[f] median of observed EF [*Dibb et al*., 2004, *Frey et al*., 2009, *Mayewski and Legrand*, 1990, *Rothlisberger et al*., 2000].

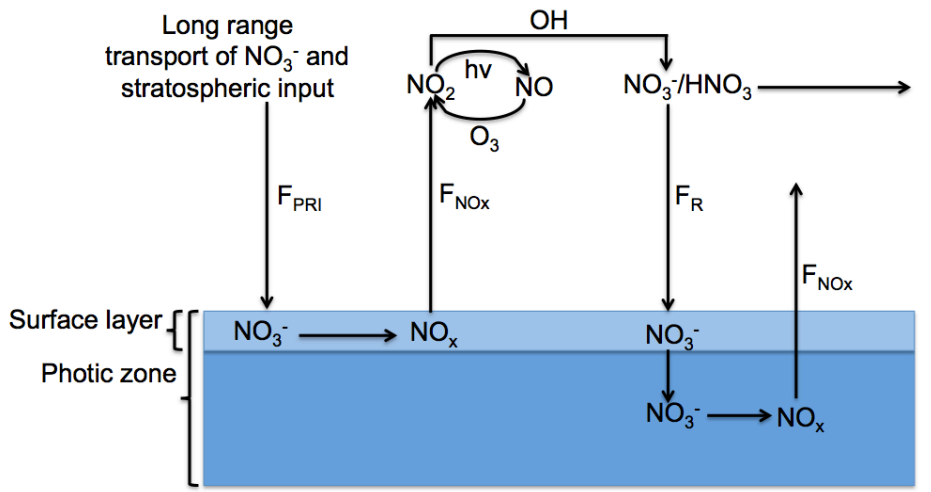

Figure 1. Schematic showing the nitrogen recycling associated with NO_3^- photolysis as included in the model. F_{PRI} (ng N m^{-2} yr^{-1}) is the downward, primary flux of NO_3^- to Antarctica originating from long-range transport and the stratosphere, F_{NOx} (ng N m^{-2} yr^{-1}) is the upward flux of snow-sourced NO_x to the boundary layer, and F_R (ng N m^{-2} yr^{-1}) is downward, recycled flux of HNO_3 to the snow surface. The surface snow layer (top 2 cm) is distinguished from the rest of the photic zone because 30-65% of snow-sourced NO_x is produced in the top 2 cm of snowpack [*Zatko et al.*, 2013], and because both NO_3^- concentrations and actinic flux are much higher in the top surface layer compared to deeper layers.

Unknown
Formatted: Font:(Default) Times New Roman

Maria Zatko 10/12/15 6:44 PM
Deleted: . ... [8]

Unknown
Formatted: Font:(Default) Times New Roman

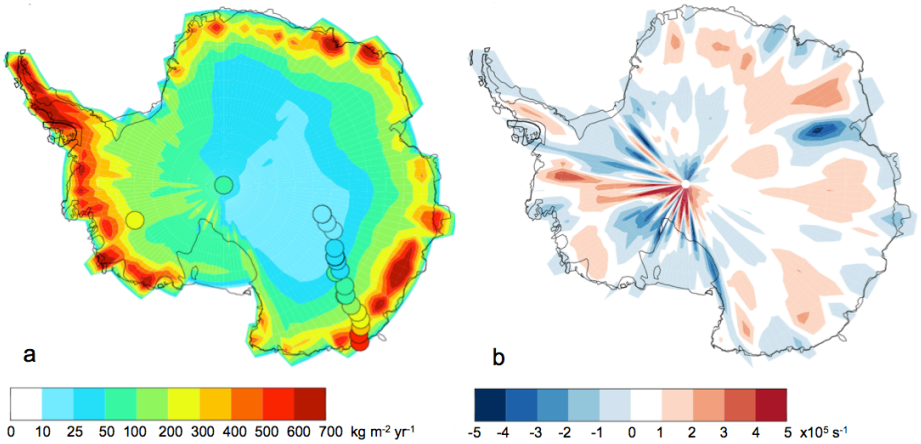

Figure 2. (a) Annual total snow accumulation rate (kg m^{-2} yr^{-1}) in GEOS-Chem from May 2009 to May 2010 with annual snow accumulation rates (circles) estimated in Erbland et al. [2013], Fegyveresi et al. [2011], and Grenfell et al. [1994]. (b) Annual mean surface wind divergence (s^{-1}) in GEOS-Chem from May 2009 to May 2010. Blue regions indicate regions of convergence.

Maria Zatko 10/14/15 4:11 PM
Deleted: , and Sofen et al. [2014].

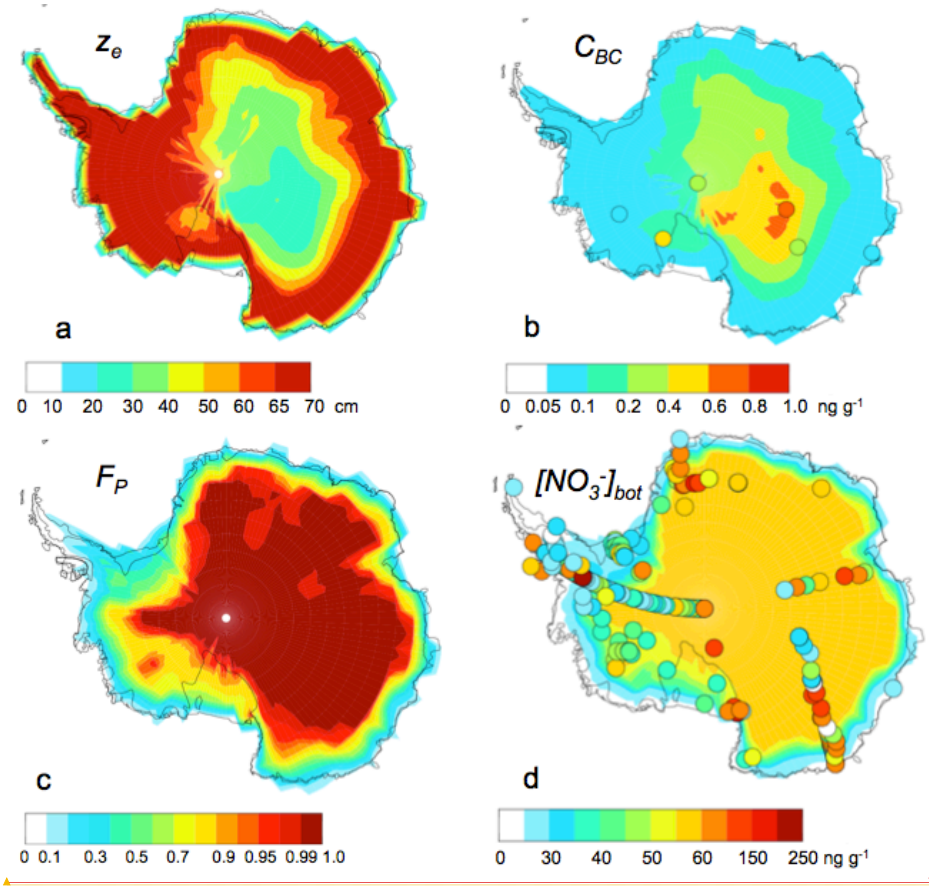

Figure 3. (a) Calculated mean austral summer (DJF) UV e-folding depth (z_e). (b) Modeled and observed (circles) annual mean snow black carbon concentrations (C_{BC}), with observations from WAIS-Divide and Law Dome [*Bisiaux et al.*, 2013], Siple Dome [*Chylek et al.*, 1992], Vostok [*Grenfell et al.*, 1994], South Pole [*Warren and Clarke*, 1990], and Dome C [*Warren et al.*, 2006]. (c) Ratio of annual dry-deposited NO_3^- to annual total deposited NO_3^-, F_P. (d) Annual sub-surface snow NO_3^- concentrations ($[NO_3^-]_{bot}$) from 2-cm depth to the bottom of the snow photic zone (z_{3e}) used in the model scaled by F_P. Mean sub-surface multi-year NO_3^- observations from the ITASE campaign along with mean asymptotic (sub-photic zone) NO_3^- mixing ratios from Erbland et al. [2013] and Shi et al. [2014] (circles) are also included in Figure 3d [*Bertler et al.*, 2005].

Maria Zatko 10/12/15 6:29 PM

Deleted:

Unknown

Formatted: Font:(Default) Times New Roman

Maria Zatko 9/11/15 8:58 AM

Deleted: along with

Maria Zatko 9/11/15 8:58 AM

Deleted: average

Maria Zatko 9/11/15 8:58 AM

Deleted: d

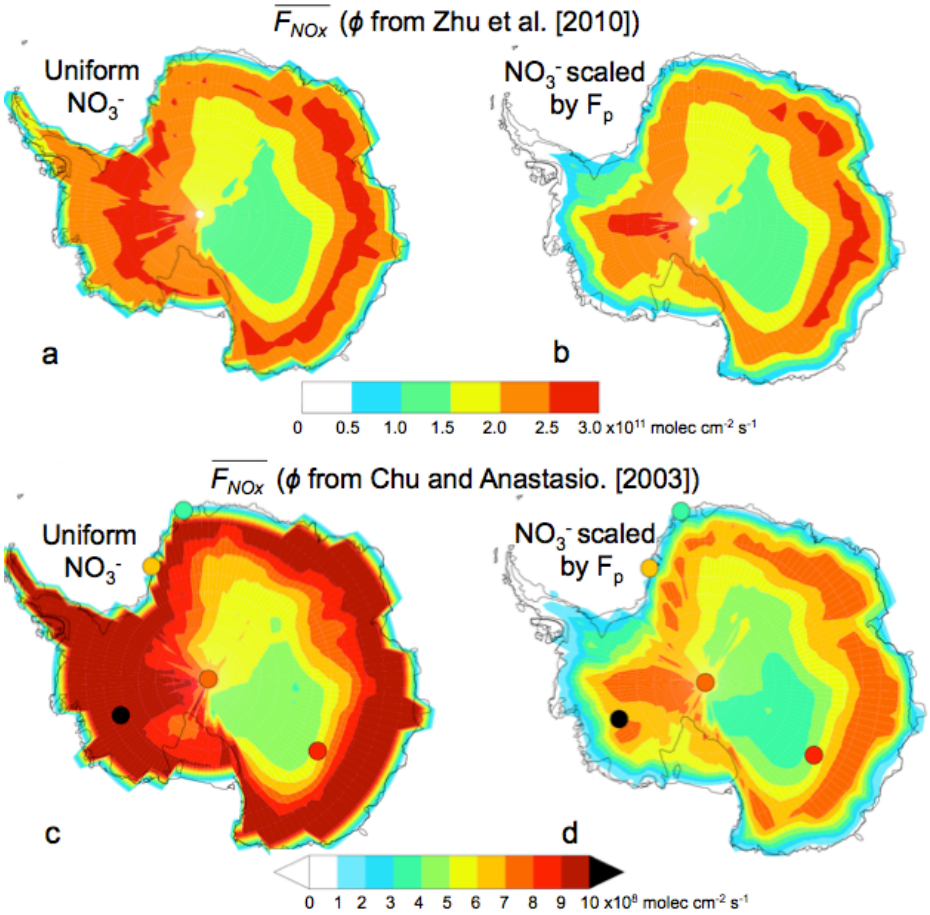

Figure 4. Mean austral summer (DJF) flux of snow-sourced NO_x from the snow ($\overline{F_{NOx}}$) with previously reported F_{NOx} observations from Neumayer [*Jones et al.*, 2001], Halley [*Jones et al.*, 2011, *Bauguitte et al.*, 2012], South Pole [*Oncley et al.*, 2004, *Wang et al.*, 2008, Zatko et al., 2013], WAIS-Divide [*Masclin et al.*, 2013], and Dome C [*Frey et al.*, 2013, Zatko et al., 2013]. (a) $\overline{F_{NOx}}$ calculated using ϕ from Zhu et al. [2010] and uniform snow NO_3^- concentrations ($[NO_3^-]_{top}$=360 ng g^{-1}, $[NO_3^-]_{bot}$=60 ng g^{-1}). (b) $\overline{F_{NOx}}$ calculated using ϕ from Zhu et al. [2010] and uniform snow NO_3^- concentrations ($[NO_3^-]_{top}$=360 ng g^{-1}, $[NO_3^-]_{bot}$=60 ng g^{-1}) scaled by the ratio of annual dry-deposited NO_3^- to annual total deposited NO_3^- (F_p, Figure 3c) (c) $\overline{F_{NOx}}$ calculated using ϕ from Chu and Anastasio [2003] and uniform snow NO_3^- concentrations ($[NO_3^-]_{top}$=360 ng g^{-1}, $[NO_3^-]_{bot}$=60 ng g^{-1}). (d) Base case: $\overline{F_{NOx}}$ calculated using ϕ from Chu and Anastasio [2003] and uniform snow NO_3^- concentrations ($[NO_3^-]_{top}$=360 ng g^{-1}, $[NO_3^-]_{bot}$=60 ng g^{-1}) scaled by the ratio of annual dry-deposited NO_3^- to annual total deposited NO_3^- (F_p).

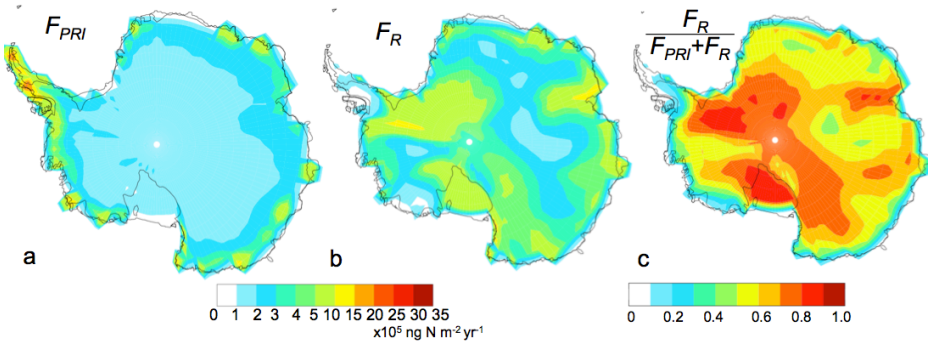

Figure 5. (a) Annual wet plus dry deposition flux of primary NO_3^- to the snow (F_{PRI}). (b) Annual wet plus dry deposition flux of recycled NO_3^- to the snow (F_R). (c) Ratio of F_R to the total downward NO_3^- flux ($\frac{F_R}{F_{PRI}+F_R}$) for the base case scenario.

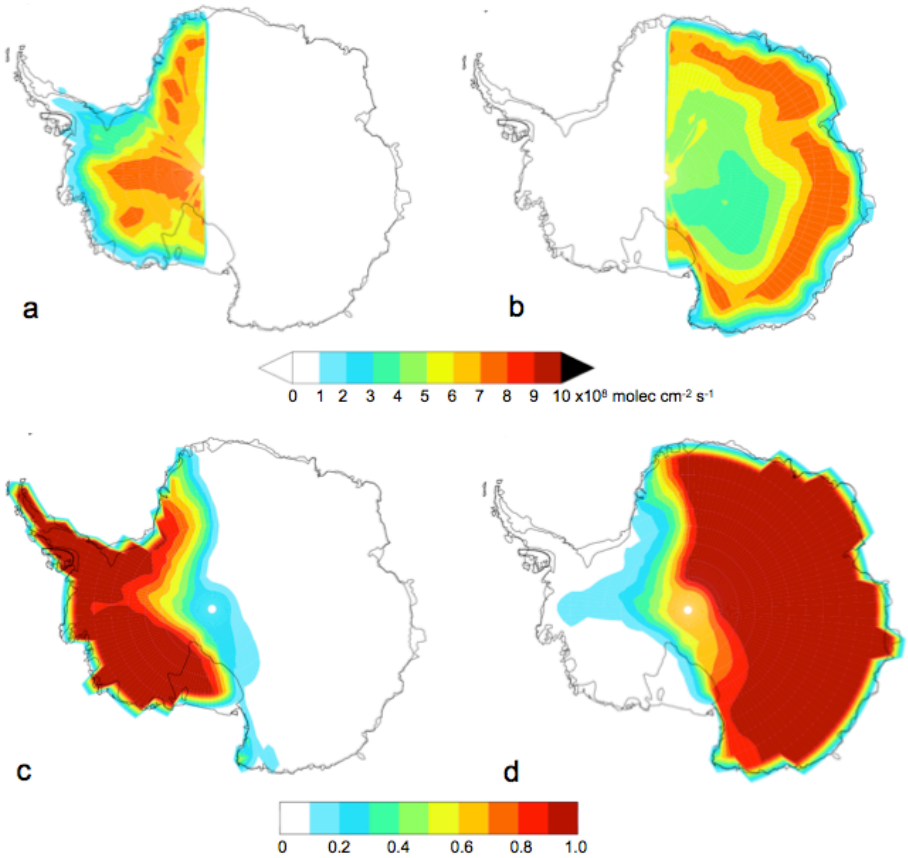

Figure 6. Sensitivity studies examining transport of snow-sourced NO_x across Antarctica. Mean austral summer (DJF) $\overline{F_{NOx}}$ across Antarctica when $\overline{F_{NOx}}$ set to 0 (a) in East Antarctica and (b) in West Antarctica. Ratio of recycled NO_3^- flux (F_R) to F_R in the base case scenario when F_{NOx}=0 in (c) East Antarctica and (d) in West Antarctica.

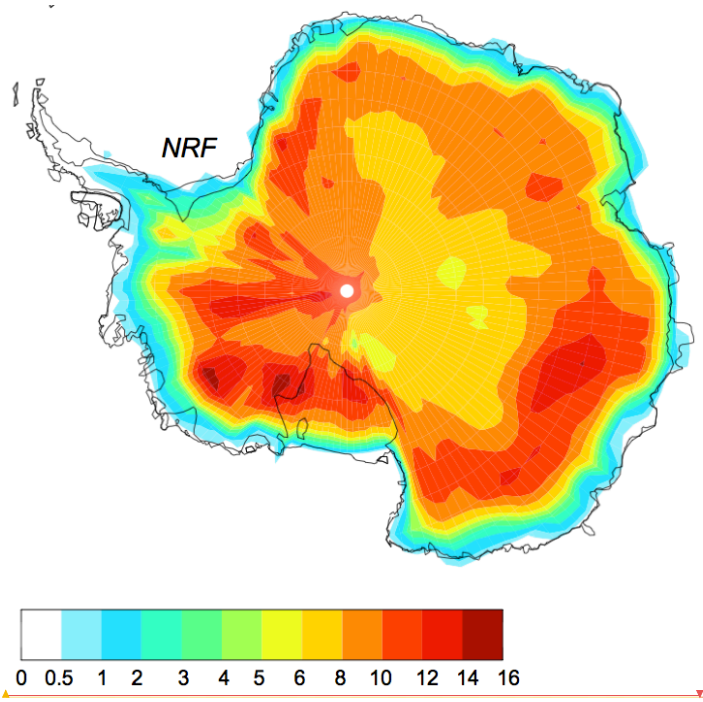

Figure 7. Nitrogen recycling factor (*NRF*, E8).

Unknown
Formatted: Font:(Default) Times New Roman

Maria Zatko 10/14/15 8:55 AM

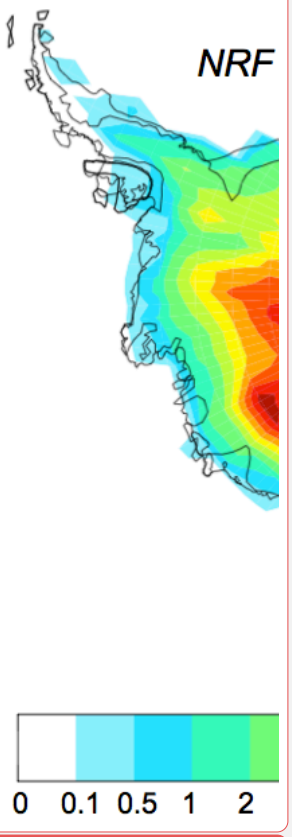

Deleted:

Maria Zatko 10/13/15 10:22 AM
Deleted: *yr*

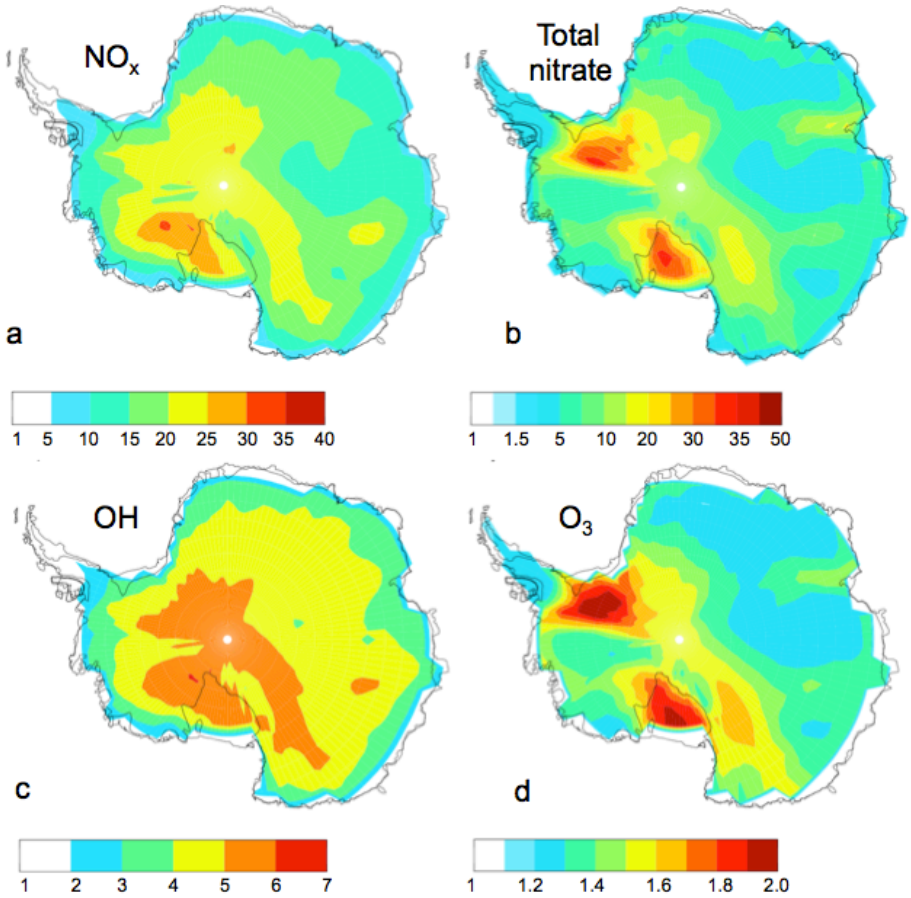

Figure 8. Factor increase in mean austral summer (DJF) boundary layer (a) NO_x, (b) gas+aerosol phase nitrate, (c) OH, and (d) O_3 mixing ratios between model runs with F_{NOx} compared to without F_{NOx}.

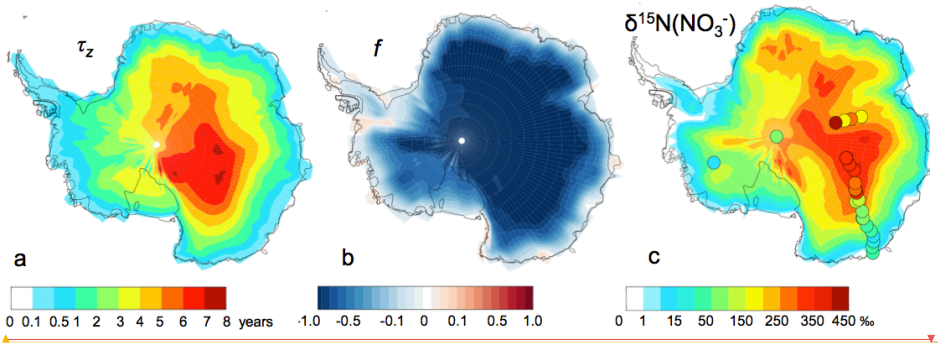

Figure 9. (a) Minimum years NO_3^- remains in photolytic zone (τ_z, years, E10). (b) Fraction of NO_3^- gained (positive values) or lost (negative values) from the snow through photolysis (f, E9). (c) Modeled enrichment in ice-core $\delta^{15}N(NO_3^-)$ (E11) due to photolysis-driven loss of NO_3^- in snow compared to sub-photic zone $\delta^{15}N(NO_3^-)$ observations [*Erbland et al.*, 2013, *Frey et al.*, 2009, *Jarvis*, 2008, *Shi et al.*, 2014, *Sofen et al.*, 2014].

Unknown
Formatted: Font:(Default) Times New Roman

Maria Zatko 10/13/15 8:02 AM

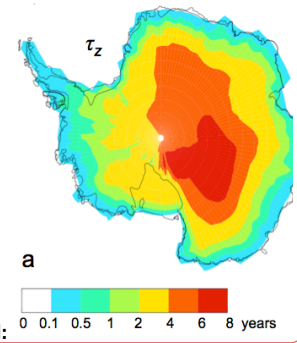

Deleted:

Maria Zatko 9/12/15 5:43 PM
Deleted: lost

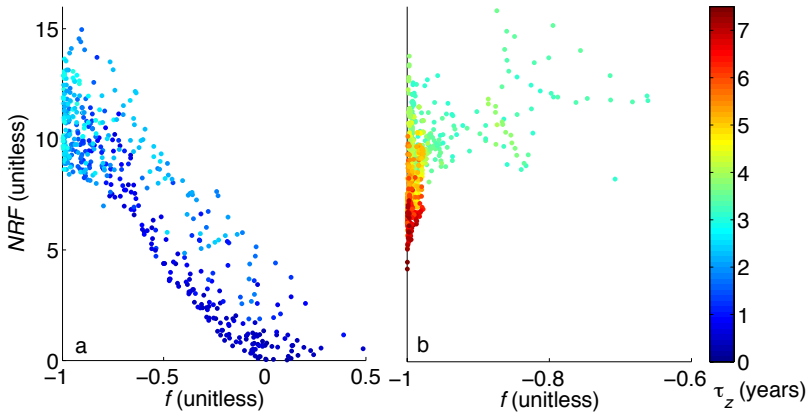

Figure 10. *NRF* versus *f* values across Antarctica. (a) Regions where NO_3^- remains in the photic zone for 3 years or less. (b) Regions where NO_3^- remains in the photic zone for more than 3 years. The color scale represents the number of years NO_3^- remains in the photic zone (τ_z). Note the different x-axis range for (a) and (b).

Maria Zatko 10/14/15 9:45 AM

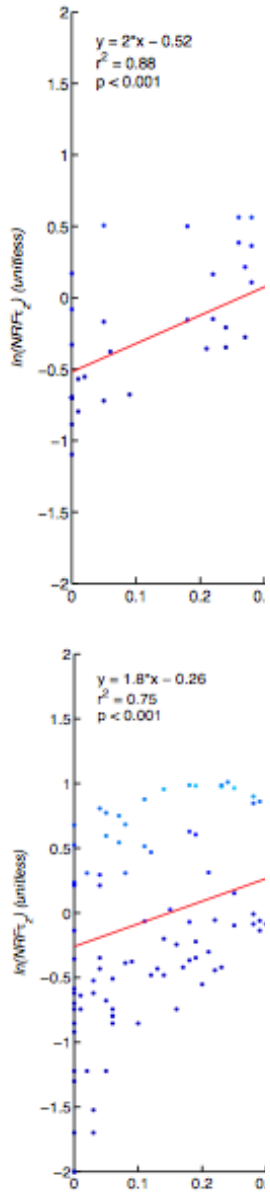

Deleted:

Unknown

Formatted: Font:(Default) Times New Roman

Maria Zatko 10/14/15 9:46 AM

Deleted: The linear regression line, r^2, and p value for all Antarctica data (East Antarctica + West Antarctica) is y=1.8x – 0.32, 0.80, and 0.001, respectively.

Appendix A

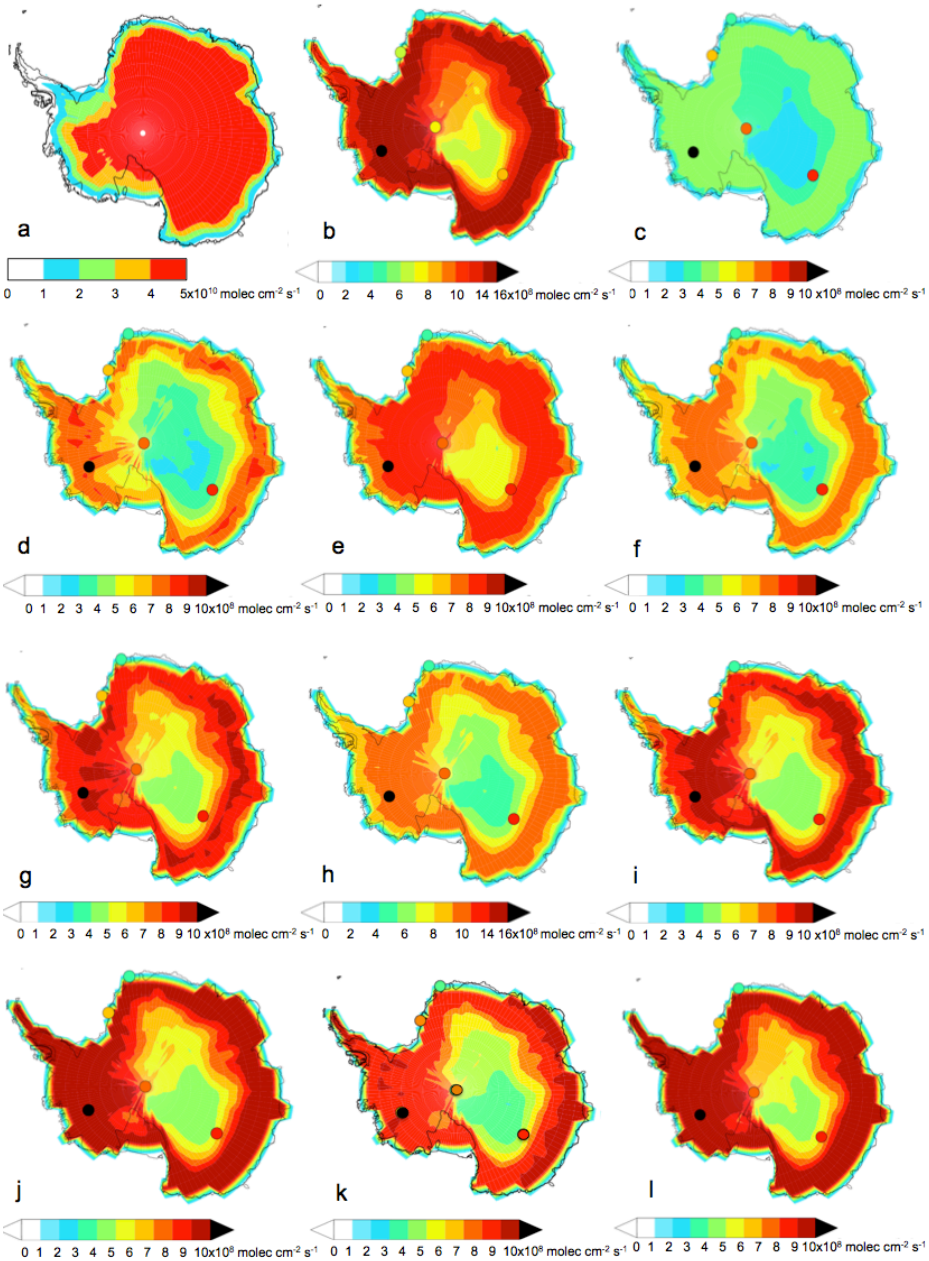
a
0 1 2 3 4 5x10^10 molec cm^-2 s^-1
b
0 2 4 6 8 10 14 16x10^8 molec cm^-2 s^-1
c
0 1 2 3 4 5 6 7 8 9 10 x10^8 molec cm^-2 s^-1
d
0 1 2 3 4 5 6 7 8 9 10x10^8 molec cm^-2 s^-1
e
0 1 2 3 4 5 6 7 8 9 10x10^8 molec cm^-2 s^-1
f
0 1 2 3 4 5 6 7 8 9 10x10^8 molec cm^-2 s^-1
g
0 1 2 3 4 5 6 7 8 9 10 x10^8 molec cm^-2 s^-1
h
0 2 4 6 8 10 14 16x10^8 molec cm^-2 s^-1
i
0 1 2 3 4 5 6 7 8 9 10 x10^8 molec cm^-2 s^-1
j
0 1 2 3 4 5 6 7 8 9 10x10^8 molec cm^-2 s^-1
k
0 1 2 3 4 5 6 7 8 9 10x10^8 molec cm^-2 s^-1
l
0 1 2 3 4 5 6 7 8 9 10x10^8 molec cm^-2 s^-1

Figure 1A. Results of sensitivity studies that show how the average austral summer (DJF) flux of snow-sourced NO_x ($\overline{F_{NOx}}$) in Antarctic snowpacks is altered by changes in variables relevant to snow NO_3^- photolysis. The standard set of variables in the above figures are quantum yield (ϕ) = 0.002 molec photon^{-1}, fraction of photolabile NO_3^- (F_p) = 1, annual mean sub-surface snow NO_3^- ($[NO_3^-]_{bot}$) = 60 ng g^{-1}, radiation equivalent mean ice grain radii (r_e) = 332 µm, NO_3^- enhancement factor (EF) = 6, bulk snow extinction coefficient ($Kext_{tot}$) = 1.7x10^{-3} to 6.9x10^{-3} (spatial variability), and annual mean snow black carbon (C_{BC}) = 0.08 to 0.6 ng g^{-1} (spatial variability). Observed $\overline{F_{NOx}}$ values are overplotted (see Figure 4 for references). In (a), for the top centimeter of snow, the Zhu et al. [2010] ϕ is applied to all dry-deposited NO_3^- and the Chu and Anastasio [2003] ϕ is applied to all wet-deposited NO_3^-. Below 1 cm, the Chu and Anastasio [2003] ϕ is applied to all NO_3^-. In (b), $[NO_3^-]_{bot}$ is doubled from the base case value and in (c), $[NO_3^-]_{bot}$ is halved from the base case value. In (d), the C_{BC} is doubled from base case values and in (e) the C_{BC} is halved from base case values. In (f), EF=1 and in (g), EF=10. In (h), $Kext_{tot}$ is a factor of 1.2 higher than the base case value. In (i), $Kext_{tot}$ is a factor of 0.8 than the base case value. In (j), r_e is representative of austral mid-summer (January) conditions is used (see Table 3 footnote). In (k), r_e is representative of austral spring, fall, and winter (March-November) conditions. In (l), r_e is representative of austral early summer and late summer (December, February) conditions. Note different color scales.